A&A 445, 1069–1080 (2006)
DOI: 10.1051/0004-6361:20053208

Astronomy & Astrophysics

Infrared photometry and evolution of mass-losing AGB stars⋆

I. Carbon stars revisited

R. Guandalini[1], M. Busso[1], S. Ciprini[2,1], G. Silvestro[3], and P. Persi[4]

[1] Dipartimento di Fisica, Università di Perugia, via A. Pascoli, 06123 Perugia, Italy
e-mail: roald.guandalini@fisica.unipg.it
[2] Tuorla Astronomical Observatory, University of Turku, Väisäläntie 20, 21500 Piikkiö, Finland
e-mail: stefano.ciprini@utu.fi
[3] Dipartimento di Fisica Generale, Università di Torino, via P. Giuria 1, 10125 Torino, Italy
e-mail: silvestro@ph.unito.it
[4] Istituto di Astrofisica Spaziale e Fisica Cosmica, 00100 Roma, Italy
e-mail: persi@rm.iasf.cnr.it

Received 7 April 2005 / Accepted 12 September 2005

ABSTRACT

As part of a reanalysis of galactic Asymptotic Giant Branch (AGB) stars at infrared (IR) wavelengths, we discuss a sample (357) of carbon stars for which mass loss rates, near-IR photometry and distance estimates exist. For 252 sources we collected mid-IR fluxes from the MSX (6C) and the ISO-SWS catalogues. Most stars have spectral energy distributions up to 21 μm, and some (1/3) up to 45 μm. This wide wavelength coverage allows us to obtain reliable bolometric magnitudes. The properties of our sample are discussed with emphasis on ∼70 stars with astrometric distances. We show that mid-IR fluxes are crucial to estimate the magnitude of stars with dusty envelopes. We construct HR diagrams and show that the luminosities agree fairly well with model predictions based on the Schwarzschild's criterion, contrary to what is widely argued in the literature. A problem with the brightness of C stars does not appear to exist. From the relative number of Mira and Semiregular C-variables, we argue that the switch between these classes is unlikely to be connected to thermal pulses. The relevance of the two populations varies with the evolution, with Miras dominating the final stages. We also analyze mass loss rates, which increase for increasing luminosity, but with a spread that probably results from a dependence on a number of parameters (like e.g. different stellar masses and different mechanisms powering stellar winds). Instead, mass loss rates are well monitored by IR colours, especially if extended to 20 μm and beyond, where AGB envelopes behave like black bodies. From these colours the evolutionary status of various classes of C stars is discussed.

Key words. stars: mass-loss – stars: AGB and post-AGB – stars: carbon – infrared: stars

1. Introduction

Winds from AGB stars replenish the Interstellar Medium with a large portion of the matter returned from stellar evolution (70% according to Sedlmayr 1994), through the formation of cool envelopes (Winters et al. 2002, 2003) where dust grains condense (Schirrmacher et al. 2003; Carciofi et al. 2004). Such grains carry the signature of the nucleosynthesis episodes occurring in the AGB phases (Busso et al. 1999; Wasserburg et al. 2005); their presence has been recognized in meteorites and brings direct information on circumstellar processes (e.g. Zinner 2000; Ott 2001). As AGB stars radiate most of their flux at long wavelengths, large surveys of infrared (IR) observations play a fundamental role in studying their luminosity and their winds (see e.g. Habing 1996; Epchtein 1999).

We do not have yet a quantitative description of AGB winds, though attempts at modelling them are a few decades old (Salpeter 1974; Knapp & Morris 1985; Gail & Sedlmayr 1987). More recently, hydrodynamical and phenomenological studies of pulsating stellar atmospheres and of the associated mass loss have undergone important improvements (Fleischer et al. 1992; Wood & Sebo 1996; Winters et al. 2002, 2003; Wachter et al. 2002; Sandin & Höfner 2003a,b). Also, observational works have become more quantitative (Wood 2003; Olivier & Wood 2003; Wood et al. 2004; Andersen et al. 2003), using new data at long wavelengths from space and from the Earth (see e.g. Wood & Cohen 2001; Le Bertre et al. 2001, 2003; Groenewegen et al. 2002a,b; Olofsson et al. 2003; Cioni et al. 2003; Omont et al. 2003), as well as improved knowledge of stellar distances (e.g. Van Eck et al. 1998; Knapp et al. 2003; Bergeat & Chevallier 2005).

A real step forward would be to derive realistic formulae, linking the efficiency of stellar winds to the luminosities,

⋆ Tables 1 to 4 are only available in electronic form at http://www.edpsciences.org

colours and chemical properties of AGB stars, to be adopted as inputs for stellar models, thus avoiding free parameterizations. This kind of studies has become quantitative only recently (van Loon et al. 2005), while previous attempts (Vassiliadis & Wood 1993; Blöcker 1995) suffered from large uncertainties (Wood 1996).

Reducing those previous uncertainties also requires a good knowledge of absolute magnitudes, through improved distances; so far, mass loss studies for galactic AGB stars often adopted some *average* constant value for the luminosity (see Jura 1986; Jura & Kleinmann 1989; Le Bertre et al. 2001). Relevant exceptions exist, e.g. in the thorough analysis of C-rich sources by Bergeat and his group (see Bergeat et al. 2002a,b, hereafter BKR1, BKR2), where however the photometric data are rather heterogeneous (see also Knapik et al. 1999; Bergeat et al. 2001).

With the above difficulties in mind, we plan to perform a thorough reanalysis of AGB luminosities and mass loss: this is actually the main scientific scope of our project for putting an IR telescope (the International Robotic Antarctic Infrared Telescope) in Antarctica, at the Italian-French base of Dome C (Tosti et al. 2004). It will allow extensive monitoring of AGB sources in Magellanic Clouds and in the southern Milky Way up to 20 μm (and possibly beyond, given the unique characteristics of the Antarctic atmosphere). This paper is in fact part of the preliminary works necessary to define the key projects for the telescope.

We shall therefore consider, in a series of works, all types of AGB stars (M, MS-S, C giants), using existing catalogues of IR observations and compiling a homogeneous list of luminosities, distances, mass loss rates, looking for correlations between them and the IR data. We start with C-rich AGB stars; next steps will analyze MS-S giants, where C- and *s*-element enrichment becomes observable, and finally the more disperse family of M giants.

In this note we collected a sample of 357 C-rich sources with near-infrared (IR) photometry and mass loss estimates; these last are revised by scaling previous observations with updated distance determinations. For another sample of 252 C stars we have collected also space-borne mid-IR photometry in the $\lambda = 8{-}15\,\mu$m interval and/or at $\lambda \sim 21\,\mu$m. The intersection of these two groups is made of 214 C-rich objects. For this sample, near IR data are provided by ground-based surveys like 2MASS (Cutri et al. 2003) and DENIS (Epchtein et al. 1999; Fouqué et al. 2000); those for mid-IR are taken from the recent space-borne missions, ISO and MSX. The relevance of MSX colours for classifying AGB stars has been recently pointed out (Ortiz et al. 2005), with an approach which is complementary to ours. IRAS measurements are not included in our analysis because of their lower quality and spatial resolution (hence larger contamination) compared to more modern experiments. A homogeneous compilation of IR colours for stars of known distance will allow us to precisely estimate the bolometric corrections (BCs) and to correlate mass loss rates with luminosity (and/or the colour excess).

We started from previous work done by BKR1 and BKR2, who classified C stars in several discrete families: the more advanced subclasses, named "Carbon Variables" or CVs, from CV3 on, correspond to bright thermally pulsing AGB stars. Bolometric magnitudes were estimated by those authors using optical photometry by Baumert (1972), near-IR data from Gezari et al. (1993), and including IRAS fluxes at 12 and 25 μm. Careful upgrades of Hipparcos were included. In our work we shall consider newer and more homogeneous IR data from the ground and from space, with Spectral Energy Distributions (SEDs) covering a wider wavelength baseline up to 45 μm. In this way we also aim at verifying on wider statistics suggestions previously advanced by Busso et al. (1996), Marengo et al. (1997, 1999), Busso et al. (2001), according to which mid-IR colours are good indicators of the mass loss efficiency, and permit a first classification of the chemical properties of the circumstellar envelopes.

The choice of discussing first a sample of Carbon-rich AGB stars is motivated by the fact that optical C(N) stars (usually irregular or semi-regular pulsators) present a sufficient level of homogeneity to be considered as a snapshot on the relatively long ($1{-}3\times10^6$ yr) TP-AGB evolution. They correspond to the moment in which the C/O number ratio reaches unity in stars of moderate mass (lower than 3 $M_\odot$: Claussen et al. 1987; Busso et al. 1999; Abia et al. 2001, 2002; Kahane et al. 2000). When looking at IR properties, however, one has to remember that more massive and evolved sources become part of the sample, thus making the picture more complex (Barnbaum et al. 1991). Mass loss rates have been shown to span a wide interval, from a few 10^{-8} $M_\odot$/yr, (Olofsson et al. 1993a,b; Schöier & Olofsson 2001) to 10^{-4} $M_\odot$/yr for the most massive and/or evolved objects (Groenewegen et al. 2002a,b).

All stars outside the mass range in which C-rich atmospheres are formed will reach the final stages while remaining O-rich. This is due either to the inefficiency of dredge-up (for lower masses), or to the fact that massive AGB stars ($M \geq 5\ M_\odot$) burn the new carbon as soon as it is dredged to the envelope, thanks to the hot bottom burning (hbb) phenomenon (Karakas & Lattanzio 2004). Observational evidence of this occurrence is emerging in various contexts (Smith et al. 1995; van Loon et al. 2001, 2005; Whitelock et al. 2003; Cioni et al. 2003). See in particular van Loon et al. (1999a,b), hereafter VL1, VL2. This paper is organized as follows. In Sect. 2 the C-star sample and the photometric measurements are presented; in Sect. 3 we discuss mass loss rates from radio studies, together with the required updates (e.g. on the distance). The luminosities and colours of our sample stars are presented in Sects. 4 and 5, together with the consequences of our analysis for the AGB evolution and dredge up. Correlations found between luminosity, colours and mass loss rates are reviewed in Sects. 6. Some general conclusions are drawn in Sect. 7.

2. C-star photometry from ISO-SWS and MSX catalogues

Ground-based photometric studies of C stars in the 8–14 μm window were often performed through 1 μm-wide filters, centered around 8.8, 11.7 and 12.5 μm. We decided therefore to compile colours including filters as close as possible to the above ones, to make comparisons easier.

The largest inventories of IR observations longward of 2.2 μm for AGB stars come from space experiments. Le Bertre et al. (2001, 2003) examined the sample from the Japanese experiment IRTS. We shall consider instead data from the European ISO mission and from the American MSX satellite (using the Infrared Point Source Catalogue, version 6C). In the case of ISO, the best known, nearby AGB stars are always too bright to be observed by the imaging camera (ISOCAM: see Cesarsky et al. 1996). Luckily, the database of the Short Wavelength Spectrometer (SWS: Valentijn et al. 1996) contains spectra of many known AGBs, and offers also a good photometric calibration. We therefore performed a re-binning of AGB SWS spectra from the ISO archives at the *Centre de Données Stellaires (CDS)* of Strasbourg. In doing this, the spectral energy distributions were convolved with the response curves of common filters centered at 8.8, 11.7 and 12.5 μm, available from the TIRCAM consortium (Persi et al. 1994). For the sake of simplicity, these filters will be indicated by: [8.8], [11.7], [12.5]. We also rebinned data at longer wavelength, convolving them with the filters at 14.7 and 21.3 μm from MSX. Sources for which ISO fluxes in different epochs vary significantly were combined to get average spectra: a few sources showed the remarkable property of a global (bolometric) variation up to a factor of two. Such phenomena have been observed previously (Le Bertre 1992, 1993; van Loon et al. 1998): for interpretations the reader is referred to van Loon et al. (1998).

A number of our sources have complete SWS spectra up to 45 μm: those among them that also have near-IR photometry and estimates for mass loss and distance (49 in total of the about 70 astrometric sources) represent a "best selection", from which we can expect to derive all photometric properties with high precision, including the bolometric magnitudes (these last will simply come out from integrating the flux from 1 to 45 μm, as for the whole sample optical fluxes are very small compared to the IR ones). Three examples of such complete spectra, representative of stars with small, moderate and large IR excess, are presented in Fig. 1. They show one of the main points we want to underline in this work: deriving bolometric magnitudes from too short wavelengths can be very misleading, especially for very red sources. As examples, using BCs derived from $J-K$, as in Costa & Frogel (1996), the sources in Fig. 1 would be assigned absolute magnitudes of: −4.8 (TX Psc); ≥1.0 (IZ Peg); ≥1.0 (V353 Aur). The last two numbers derive from assuming generous upper limits of 0.05 Jy for the very low J fluxes of these red sources. When BCs are instead computed starting from IR photometry extending from the K-band to 10–20 μm, as in Le Bertre et al. (2001), more reasonable magnitudes are obtained: $M_{\rm bol} = -5.2, -4.8, -5.9$, respectively. When, finally, we apply our BCs (see next sections) derived from photometry up to 45 μm, we get $M_{\rm bol} = -5.5, -4.8, -6.2$ in the three cases. For very red sources (about 25% of Miras and most post-AGBs) even our Spectral Energy Distributions (SEDs) up to 45 μm are insufficient to gather the whole flux. For them, the luminosities we estimate will be lower limits.

Concerning the MSX sample, we adopted the fluxes at 14.7 and 21.3 μm as provided by the catalogue, while in the 8–14 μm range, fluxes in the [8.8] and [12.5] filters were inferred from

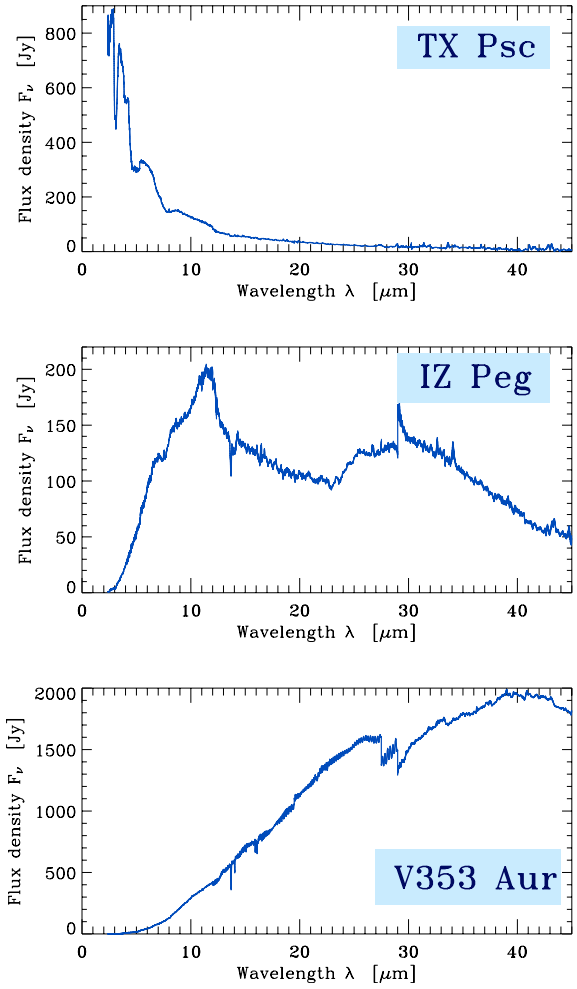

Fig. 1. SWS spectra for an irregular variable (TX Psc), a Mira variable (IZ Peg) and a post-AGB star (V353 Aur). The dominant role of IR emission longward of 20 μm for Miras and post-AGB sources is a general property of our sample.

those in the MSX bands "A" and "C". In order to do this we selected a group of sources in common between ISO-SWS and MSX. For them, we derived correlations between the two sets of filters, obtaining the following relations:

$$\log F_{12.5} = 0.80176\ \log F_C + 0.3349$$

$$\log F_{8.8} = 0.9377\ \log F_A + 0.1266$$

with regression coefficients (R^2) of 0.95, 0.94 respectively. The relations apply to all sources examined: colour effects on different types of stars are negligible. They were used for expressing the MSX fluxes in the set of filters adopted. This can be done without loss of accuracy, as the uncertainty of IR colours is at least $\pm 0.1^{\rm m}$. No flux at 11.7 μm can obviously be derived for MSX stars.

The resulting list of ISO and MSX C-rich AGB sources, with their inferred IR fluxes, is presented in Tables 1 to 4. Here variability types are taken from the Combined General Catalogue of Variable Stars (Samus et al. 2004). In the tables we have included near-IR data from 2MASS, together with general information available on the variability type and on parameters relevant for estimating mass loss rates (see next

section). One problem affecting our sample is that data from catalogues are single-epoch measurements; though the amplitude of the light curves decreases sharply when moving from optical to near-IR wavelengths, we expect that J, H, K data can be still affected by uncertainties of several tenths of a magnitude. This problem affects only the bluest semi-regular and irregular variables (at the lowest luminosities and mass loss rates considered). Indeed, despite the fact that redder sources also show larger amplitude variations in near-IR filters, their flux is usually dominated by mid-IR wavelengths, where the variability vanishes because the photosphere is not seen. The very large near-to-mid IR colours of several Miras and of all post-AGB sources make any variability at short wavelengths irrelevant (exceptions might occur for the few sources showing factor-of-two variations in the bolometric luminosities). Also, the photometric data in the tables do not contain corrections for interstellar extinction, for two reasons. On one side extinction becomes small at the long wavelengths considered here; on the other hand, our stars are distributed in all directions of the sky, so that we should adopt average extinction laws, but these are rather uncertain, and it is not clear that (at IR wavelengths) average corrections are substantially better than nothing. As our stars are occasionally very distant (above 1 kpc) one has to estimate the effects of neglecting extinction. Let's consider representative cases at 200 and 2000 pc distance. For the average interstellar medium one has $A_{\rm V}(200\ {\rm pc}) = 0.15^{\rm m}$; $A_{\rm V}(2000\ {\rm pc}) = 2.2^{\rm m}$ (Gillett et al. 1975; Knude 1979). The wavelength dependence can be taken from Draine (1989), as being $A_\lambda \sim \lambda^{-1.75}$. At mid-IR wavelengths (10 μm and beyond) this implies negligible corrections ($0.015^{\rm m}$ at maximum), well within the photometric uncertainly, even for the most distant sources. In the K-band (2.2 μm) extinction is irrelevant within 1 kpc, but may be appreciable for the most distant stars ($0.2^{\rm m}$ at 2 kpc). We notice that the unknown variability induces a scatter whose amplitude is similar to the uncertainty related to extinction. Neglecting this last, however, introduces systematic effects on the most distant stars, so that their near-IR luminosity will be underestimated. Hence at near-IR wavelengths, catalogue data for distant ($\geq$1 kpc) LPVs taken at face values are typically uncertain by a few tenths of a magnitude (from both statistical and systematic errors). The effects on the bolometric magnitude distribution in our sample are however small, due to the large IR excesses of most distant sources that make near-IR data relatively unimportant for them.

When using the data of Tables 1 to 4 for determining standard colours, we applied standard photometric calibrations, adopting suggestions by Bessell et al. (1998) and by Glass (1999) and interpolating them with black bodies for obtaining the fluxes in the selected 1-μm-wide filters. According to this procedure, the fluxes (Jy) of a zero-magnitude star in the filters used are: 52.23 ([8.8]), 29.55 ([11.7]), 25.88 ([12.5]), 20.25 ([14.7]), 8.91 ([21.3]). For near-IR, 2MASS calibrations are given in Cohen et al. (2003).

3. Estimates for mass loss and related problems

The work by Jura (1986) and Jura & Kleinmann (1989) set the stage for subsequent studies on AGB winds. These authors used mass loss rates estimated across the previous ten years, and mid-IR photometric observations from the IRAS satellite. Unfortunately, the scarcity of data then available led them to adopt *average* hypotheses on the luminosities, assuming a constant value of $10^4\ L_\odot$ for all types of AGB stars. This fact (and the modest precision of IRAS photometry) prevents us from making too systematic comparisons of those works with the present analysis, where the luminosities are estimated thanks to measurements of the distance, sometimes of astrometric quality. We shall however comment later on mass loss rates for the sources we have in common with the quoted studies.

The inventory of more recent analyses on mass loss in AGB stars includes works dedicated to Carbon-rich stars (Olofsson et al. 1993a,b; Kastner et al. 1993; Schöier & Olofsson 2001; Groenewegen et al. 2002a,b; Schöier et al. 2002), to oxygen-rich M–MS–S stars (Sahai & Liechti 1995; Groenewegen & de Jong 1998; Olofsson et al. 2002), and more general approaches including all classes of AGB objects (Kastner 1992; Loup et al. 1993; Le Bertre et al. 2001, 2003; Winters et al. 2002, 2003). From the theoretical point of view, the very limited evidence of coronal X-ray emission (Jura & Helfland 1984; Sahai et al. 2003; Kastner & Soker 2003) demonstrated that mass loss mechanisms were different than in the sun. Radiation pressure on dust grains was suggested to be at the origin of red giant winds by Salpeter (1974). In this approach, if the momentum of the radiation field can be completely transferred to dust and gas particles in the envelope, then the mass loss rate can be expressed as:

$$\dot{M} \sim 2 \times 10^{-8} \tau_{\rm d} (L_*/L_\odot) \times (v/{\rm km\,s^{-1}})^{-1} M_\odot/{\rm yr}$$

where $\tau_{\rm d}$ is the average optical depth of dust. The gas phase of the envelope might be dragged by dust, but a problem is how to transfer momentum to dust close to the photosphere, as above 1500–2000 K no solid compound made with light elements (C to Si) would avoid evaporation. Hence, stellar pulsation in different modes (Wood et al. 1999; Wood 2000), pushing the radius to large distances and the temperature to low values, and introducing shock waves should also be very important (see e.g. Fleischer et al. 1992, 1995; Winters et al. 1994a,b, 1997, 2000a,b).

All approaches suffer from many limitations, so that recent work was concentrated on semi-empirical approaches derived from observations. As an example, Le Bertre et al. (2001, 2003) used near-IR fluxes (in K, L'), then adopting simplifying assumptions like e.g a constant luminosity of 8000 $L_\odot$ for all the sources studied. Being based on a wavelength interval where the AGB photosphere dominates the flux, these estimates are also affected by the intrinsic uncertainty of the variability.

Other mass loss estimates were derived from observations at millimeter or radio wavelengths, where the variable star is not seen. In most cases they adopt procedures early suggested by Knapp & Morris (1985) for CO lines. For example, Olofsson et al. (1993a,b) and Groenewegen et al. (2002a,b) assume emission from an optically thick environment, with a fixed size for the CO envelope, $R_{\rm CO}$. Due to this, they can sometimes underestimate the wind efficiency by factors 3–4 (Schöier & Olofsson 2001).

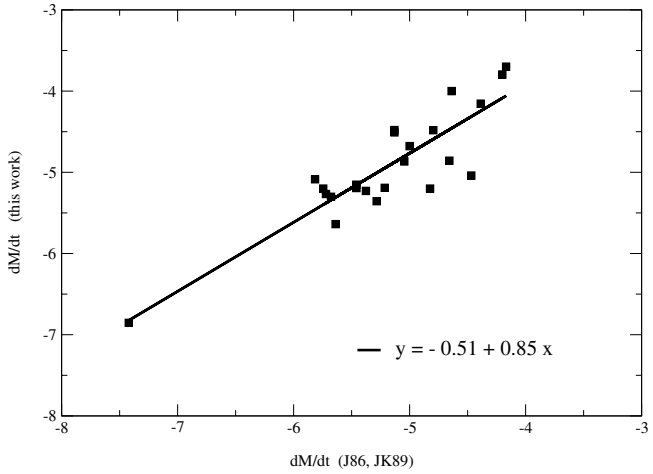

Fig. 2. The existing correlation between mass loss estimates published by Jura (1986) and Jura & Kleinmann (1989) and our re-calibration of measurements from Loup et al. (1993) with updated distances.

A more general case was considered by Loup et al. (1993), Kastner (1992), Kastner et al. (1993) and Winters et al. (2003). The results are given in terms of the distance d (in kpc), of the expansion velocity V_e (in km s^{-1}), and of the flux f. We adopt Loup et al. (1993)'s formulation whenever possible, re-scaling their mass loss rates with more recent estimates for the distance and for V_e. When data from Loup et al. (1993) are not available, we use instead the Olofsson et al. (1993a,b) procedure, again updating the parameters when possible.

Tables 1 to 4 report the relevant data for those stars for which IR photometry was derived in the previous section, together with the updated estimates for mass loss rates. It is interesting to note (see Fig. 2) that for the few sources we have in common with Jura (1986) and Jura & Kleinmann (1989) and despite the mentioned uncertainties of these older analyses, there is a fair correlation between the mass loss rates given by the above authors and those derived by us (with a regression coefficient $R^2 = 0.88$). In most cases the sources are Mira variables.

We shall be guided by the data of the AGB stars (Table 1) with the best distance estimates. They include objects with astrometric measurements (usually from Hipparcos), for which we adopt the recommended values by Bergeat & Chevallier (2005), plus a small group of post-AGB stars for which the distance was derived from dedicated studies of the circumstellar envelopes. Our mentioned "best selection" is actually made by those sources, among the objects in Table 1, for which also the integral of the SED up to 45 μm is available. We give a lower weight to other methods of deriving distances (the corresponding points in the figures will be smaller). When nothing else is available, we quote in the tables distances estimated by Loup et al. (1993) by assuming a specific value for the luminosity. Obviously, these sources will be used only when a precise knowledge of the distance is irrelevant, e.g. in colour–colour diagrams.

4. Energy distributions and photometric calibrations

A few SEDs, chosen to represent the various shapes found in our sample, are shown in Fig. 3. They illustrate how different the spectra for different types of sources are, displaying the increasing importance of mid-IR (10 and 20 μm) wavelengths when moving from irregular (or semi-regular) pulsators toward Miras and post-AGB stars. This has two important consequences as discussed below.

First of all, it is clear from the figure that, when the observations are not extended up to at least 20 μm, most of the flux from the reddest objects is missed. Plots like those in Fig. 1 reveal that many AGB stars radiate the majority of their flux in a region between 20 and 45 μm. This range is rarely considered in dealing with large samples of sources. In the past, the flux in the 60 μm IRAS filter was often used as representative of far IR, and correlated with mass loss. However, IRAS 60 μm data may be partially contaminated by diffuse (cirrus) emission; moreover, the IRAS spatial resolution at those wavelengths is very poor.

Secondly, when we consider the relative number of sources having SEDs with the various appearances of Fig. 3 (with semiregulars and Miras occurring with nearly equal frequency) doubts arise on the common idea that the different variability types are alternatively encountered along the AGB due to the variations of luminosity in correspondence of thermal pulses (see e.g. Cioni et al. 2001). These doubts are best illustrated with reference to the behaviour of the stellar luminosity on the AGB (Fig. 4). The usual interpretation might in principle be true for the first thermal pulses, when the star is oxygen-rich, as regimes of higher and lower luminosity are both encountered, due to the occurrence of post-flash dips. In early phases these dips cover nearly 30% of the time between adjacent pulses (for a recent review on the models, see e.g. Straniero et al. 2005) and hence imply that lower-luminosity variables (identified with semiregulars) should account for ∼30% of the total number of O-rich AGB stars. However, for the final C-rich phases the duration of low-luminosity regimes becomes increasingly short with increasing pulse number. According to Fig. 4, relative to a 2 $M_\odot$ AGB star of solar metallicity, the stages where the luminosity is lower than average by at least 0.2^m account for about 10 percent of the time spent by the star as a C-rich giant: if C-rich semiregular variables were to be associated with these low luminosity regimes, they should be pretty rare, contrary to the evidence we have. Our sample was selected from mass loss data and therefore is certainly biased toward the reddest and more mass-losing Miras, but despite this semiregular variables are of equal statistical weight. If the AGB stars really switch from one variability type to another (see e.g. Cioni et al. 2001) this is unlikely to be related to thermal pulses; rather, in atmospheres animated by complex pulsations, superposition of close-by frequencies can induce beats and hence amplitude modulations (with periods of centuries or millenia, see e.g. Marengo et al. 2001) that may be independent from what happens in the internal layers. One has to notice that, in the BKR1 & BKR2 classification in CV classes, the complex behaviour of the C/O ratio shows an increase with

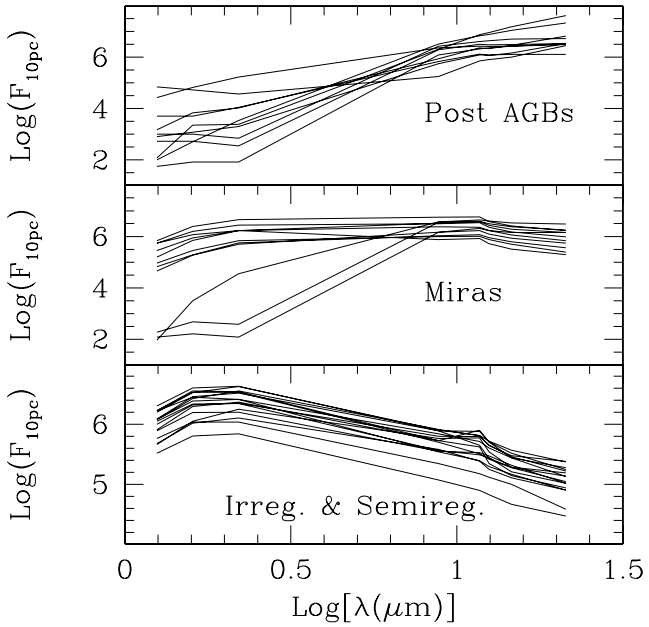

Fig. 3. The Spectral energy distribution up to 21.3 μm of a number of sources in our sample, divided according to their type, as constructed with the set of 1-μm-wide filters described in the text.

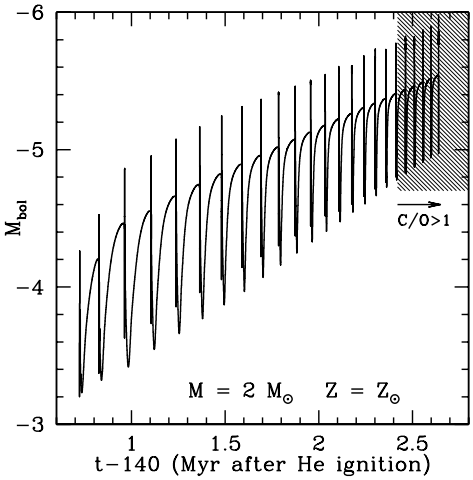

Fig. 4. Model bolometric magnitude of a 2 $M_\odot$ AGB star during the phase of thermal pulses on the AGB. Model from the FRANEC code, as computed by Straniero et al. (1998).

class number and with decreasing $T_{\rm eff}$, down to about 2500 K; Miras (classes CV5−CV6) occupy regions with higher C/O ratios than SRa,b stars (classes CV3+ and CV4). This fact, and the gradual SED changes we see (Fig. 3), with smooth transitions from Semiregulars to Miras and then to post-AGBs, leads to the conclusion that, at least on average, most Miras are in an evolutionary stage subsequent to semiregulars. Oscillations between the two types should exist, but the final evolutionary stages should be more heavily populated by Mira-like variables.

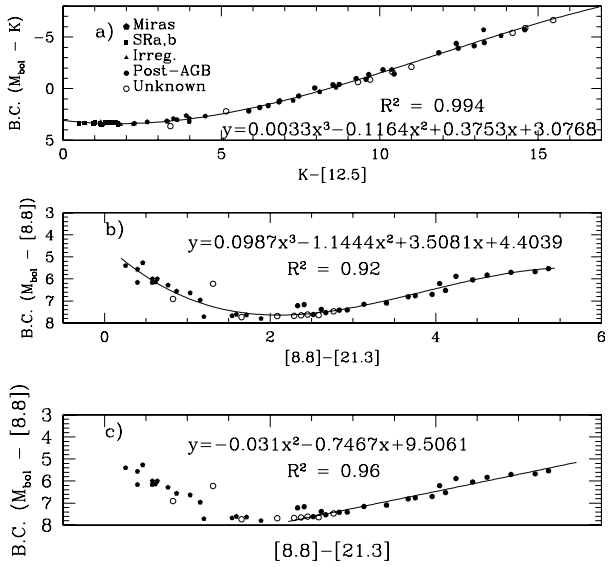

Fig. 5. a) Bolometric corrections for the K magnitude as a function of the K–[12.5] colour. They were derived for AGB C-stars with complete SEDs, from 2MASS and ISO-SWS, up to 45 μm. **b**) and **c**) Bolometric corrections for the [8.8] magnitude, as a function of the mid-IR colour [8.8]–[21.3]. Of the two relations shown, the one in **c**) is more appropriate for extrapolations to very red sources, as the cubic spline of **b**) introduces unwanted biases outside the range shown.

SEDs like those of Fig. 3 were the base for estimating bolometric magnitudes. We used for this the fundamental relation of photometry, according to which one has (see e.g. Glass 1999):

$$M_{\rm bol} = \int_0^\infty F_\nu {\rm d}\nu + C \qquad (1)$$

where $C = -18.98$ when the flux is expressed in W/m^2. As a consistency check we derived the zero-magnitude flux from the data of Bessell et al. (1998), extended from the U to the Q band, finding $C = -19.01$, a very good approximation to (1). The bolometric magnitude of AGB stars has often been derived from corrections applied to the K magnitude; these corrections are usually a function of the K–[12] colour (using e.g. IRAS data, see Le Bertre et al. 2001, 2003). For the sake of comparison, we too present here our $M_{\rm bol}$ estimates through bolometric corrections as a function of the (K–[12.5]) colour. If f is a measure of the flux in Jy (Tables 1–4):

$$K = -2.5 \times \log\ f_{\nu,K} + 5 - 5 \times \log\ d + 2.5 \times \log\ f_{\nu,K_0} \qquad (2)$$

where d is the distance in parsec and f_{ν,K_0} is the zero-magnitude flux in K.

Bolometric corrections derived from Eqs. (1) and (2) are shown in Fig. 5 (panel a) as a function of the K–[12.5] colour, together with a fitting formula for extrapolations. Optically-selected sources (in general semi-regular variables) have small corrections: their flux is well estimated from traditional criteria at short wavelengths, as most flux is radiated in near-IR. Alternative expressions of the B.C., as a function of mid-IR colours alone, to be used for very red sources too faint in near-IR, are presented in Fig. 5 (panels b, c). Here semiregular variables are omitted, because of their small IR excess (see Fig. 1).

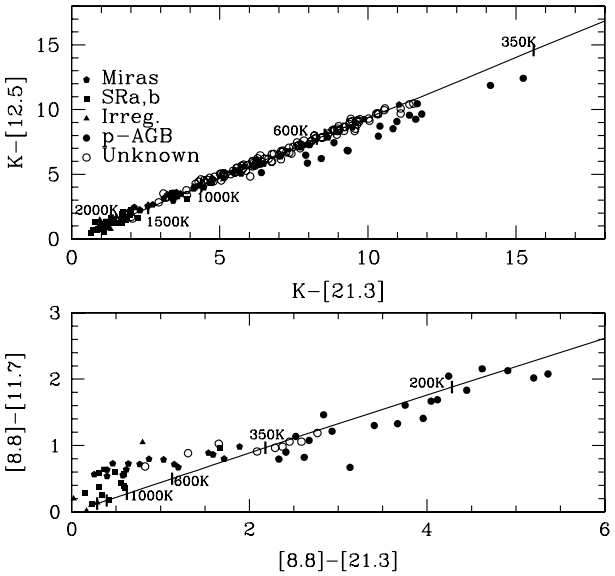

Fig. 6. Examples of colour–colour diagrams in the IR for C-rich AGB and post AGB stars.

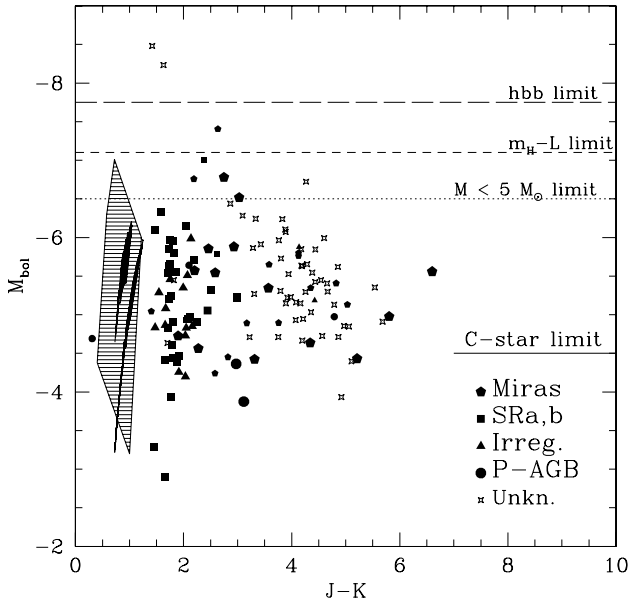

Fig. 7. The HR diagram of observed C stars in near IR, as compared to the area (dashed) covered by canonical stellar models (without hbb). The minimum limit for C star occurrence in the adopted models is indicated.

Finally, we must notice that mid-IR emission from circumstellar envelopes makes the stars of our sample appear as black bodies at long wavelengths, apart from the known typical features of C-rich dust. This is shown in Fig. 6, where calibrated colour–colour diagrams are shown for near- and mid-IR filters. In the top panel, adopting the $K-[21.3]$ colour as baseline, the data points of known AGBs and of sources (mainly from MSX) of unknown variability type are almost perfectly aligned on the blackbody sequence; they should be dominated by cool, evolved Mira stars with extended dusty envelopes; post-AGB sources instead display excess emission at 21.3 μm, which is a well-known property of such C-rich objects (van Winckel & Reyniers 2000). The bottom panel then shows that, if only mid-IR is used, including the [11.7] filter where SiC and PAH features are present, then normal AGB C stars show excesses in this filter, while post-AGB C-rich sources gradually move to an excess at 21.3 μm, while becoming redder. In general, Miras are redder than semiregulars and Post-AGBs are the reddest sources of the sample (due to their cold dust). In the evolutionary hypothesis we have tentatively advanced before (at least on average), this graph would offer an immediate tool for classifying the evolutionary status of C-rich circumstellar envelopes.

5. Bolometric magnitudes, colours and model comparisons

The magnitudes derived by our analysis are used in Fig. 7, where HR diagrams are presented, using an IR colour as abscissa. As stated, small symbols refer to stars with less-accurate distances: they are usually distant post-AGB objects, or AGBs of unknown variability type. The dashed area in Fig. 7 represents the zone covered by standard stellar models with the Schwarzschild's criterion for convection, adopting the usual mixing length theory as adapted to stellar physics by Cox & Giuli (1968). The value of the so-called parameter α (ratio of the mixing length to the pressure scale height) is $\alpha = 2.1$ (Straniero et al. 1998). All models considered are from the FRANEC evolutionary code; they refer to metallicities from $Z = Z_{\odot}/3$ to $Z = Z_{\odot}$ and include models of relatively low mass (2 to 3 $M_{\odot}$) (Straniero et al. 1997; Gallino et al. 1998; Busso et al. 1999), plus intermediate mass star models (Domínguez et al. 1999; Straniero et al. 2000). As representative cases, we plot explicitly the track of a $2M_{\odot}$ star with $Z = Z_{\odot}$, and that of a 3 $M_{\odot}$ star with $Z = Z_{\odot}/3$ (heavy lines). As compared to the evolutionary tracks, the data points (which are systematically displaced at redder colours) show the gradual formation of cool and dusty circumstellar environments, which recycle part of the stellar flux at longer wavelengths through the absorption and re-emission mechanisms of dust grains. For the bluest sources, the displacement in $J-K$ with respect to theoretical predictions might also be due to models underestimating molecular opacities of C-rich material (Marigo et al. 2003).

We underline that the models adopted do not assume any overshoot for convection (contrary to, e.g. Frost & Lattanzio 1996); for the techniques used to compute the convective border see Straniero et al. (2003). Overshooting from the convective envelope and in general an extension of dredge up larger than allowed by the Schwarzschild's criterion is even today a common assumption (Herwig 2005). This is usually claimed to be needed for letting the photospheres become C-rich *at low luminosities*, in order to fulfill constraints like those by Blanco, Blanco & McCarthy (1980) and Costa & Frogel (1996), derived by optical and near-IR data, suggesting average C-star magnitudes below −5. We notice that similar works in the optical bands became recently feasible on other galaxies, and the results were essentially the same, yielding C-star magnitudes between −4.5 and −5, again neglecting IR fluxes (Battinelli & Demers 2004a,b; Demers et al. 2004).

Despite some contrary evidence, which has emerged from IR studies of Magellanic Clouds and of the Galaxy (see van Loon et al. (1998), VL1, VL2, BKR2) some theorists assume, even today, that such faint bolometric magnitudes characterize the whole family of C-stars, and yield a disagreement with stellar models adopting the Schwarzschild's criterion (Stancliffe et al. 2005; Herwig 2005). Our data do not support this belief: Fig. 7 reveals a substantial agreement of the observed luminosities with model predictions. Indeed, observed bolometric magnitudes are mainly concentrated in the range from −4.5 to −6.4, while models find C stars for $M_{\rm bol} \leq -4.7$ at solar metallicity, and for $M_{\rm bol} \leq -4.5$ at $Z = Z_{\odot}/3$. Moreover, in commenting Figs. 1 and 3 we already noticed that the short wavelength filters are insufficient to estimate the magnitudes of red C-rich sources, enshrouded by dust. C-star bolometric magnitudes below $M_{\rm bol} = -5$ do exist in LMC (see e.g. van Loon et al. 1997), but they should not represent the *average* population. In view of the fact that optical C(N) sources always show C/O ratios close to 1, this can be easily understood in terms of evolution: subsequent phases give birth to redder objects, more C-rich (e.g. classes CV5−CV6 of BKR2), radiating their flux mainly in mid-IR and having a luminosity function shifted at higher luminosities (see e.g. VL2).

Compared to previous work on galactic C-rich giants by BKR1 and BKR2, our sample (with more homogeneous photometry and with a wider coverage of IR wavelengths) further emphasizes the importance of high luminosity C-stars. In the luminosity functions (LFs) of the above authors (see e.g. Fig. 5 of BKR1, where the CV sources with the best distances were plotted) about 43% of CV3–CV6 sources are brighter than $M_{\rm bol} = -5$, while in our sample (Fig. 8) these account for about 60% of the total sample; similarly, 33% of CV3–CV6 sources in the quoted papers lay below $M_{\rm bol} = -4$, while in our data their fractional number is about 2%. On the whole, our distribution is displaced to higher luminosities due to a higher weight of observations at long wavelengths.

Our sample of galactic stars integrates previous IR studies on dust-enshrouded C stars in LMC (van Loon et al. 1998, VL1, VL2). These works were forcedly restricted to a relatively small number of sources: in this limit, their bright LF had little overlap with the fainter one of optically-selected C stars (VL1, VL2). However, other selection criteria lead to intermediate average magnitudes (around $M_{\rm bol} = -5$: see Whitelock et al. 2003). Our Fig. 8 now shows that the LF of galactic C stars is in fact continuous, unique and quite wide. A comparison with the bottom panel shows that our global distribution looks pretty much as a superposition, with gaps filled, of LFs previously obtained for different samples of C stars in LMC.

As mentioned previously, remaining uncertainties on bolometric magnitudes for the reddest stars, for which we have sometimes an incomplete coverage of the IR flux, would further populate the high-luminosity tail of the histogram, making our conclusions even stronger. The few points we have at low luminosity ($M_{\rm bol} \geq -4$) correspond to the HC classes of BKR2. We refer to those papers for a detailed list of the possible physical mechanisms explaining them.

A few sources in Fig. 7 exceed model predictions for the luminosity. Let us discuss this in some detail. We recall that

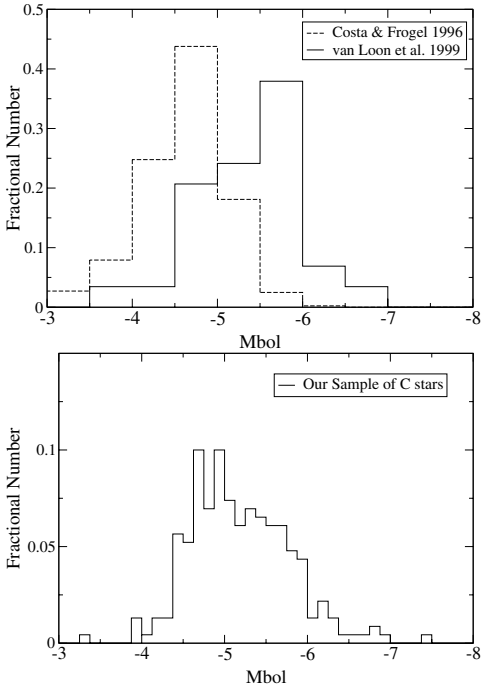

Fig. 8. *Top panel*: the histogram showing the fractional number of C stars per magnitude interval in our sample (230 sources). *Bottom panel*: same as before, for the samples of LMC C stars in optical wavelengths (Costa & Frogel 1996, 887 sources) and in the infrared (VL2, 29 sources; note that the bin size here is the same as used by these authors for their data.

a well-defined relation exists on the AGB (Paczýnski 1975; Iben & Renzini 1983; Wagenhuber & Groenewegen 1998) between the core mass ($m_{\rm H}$) and the luminosity (L). Only if $m_{\rm H}$ reaches the Chandrasekhar limit can an AGB star attain the (slightly model-dependent) limit of $-7.1^{\rm m}$. Values higher than this require an extra source of energy, as in the case of massive AGB stars ($M \geq 5\ M_{\odot}$), which develop very high temperatures at the base of the convective envelope, allowing the onset of hbb. In models by Karakas (2003), AGB stars with hbb can in fact reach $M_{\rm bol} \sim -7.75$. Normal AGB stars (i.e. without hbb) must instead remain well below the $m_{\rm H} - L$ limit, as $m_{\rm H}$ never reaches the Chandrasekhar limit, due to efficient mass loss.

This is even more true for C stars: very bright Intermediate Mass Stars ($M = 5{-}9\ M_{\odot}$) can hardly become carbon rich, even in the absence of hbb, as any ^{12}C dredged-up from He-burning layers is diluted over several solar masses of oxygen-rich material in the convective envelope (see e.g. Busso et al. 1999; Gallino et al. 1998; Abia et al. 2001, 2002).

Recently, C stars more massive than 4–5 $M_{\odot}$ have been obtained by Karakas (2003), but only for relatively low metallicities ($Z = 0.004$ to $Z = 0.008$). Such short-living stars should however be extinct by now. Formation of very bright C stars is in principle possible in the evolution of high-mass AGB objects (say, 6 to 9 $M_{\odot}$), when hbb ceases at the end, and if mass loss suitably limits the envelope mass, so that the last few thermal pulses make the photosphere become C rich (Frost et al. 1998; Karakas & Lattanzio 2003; Karakas 2003). Statistically, however, these massive C stars should be extremely rare, both

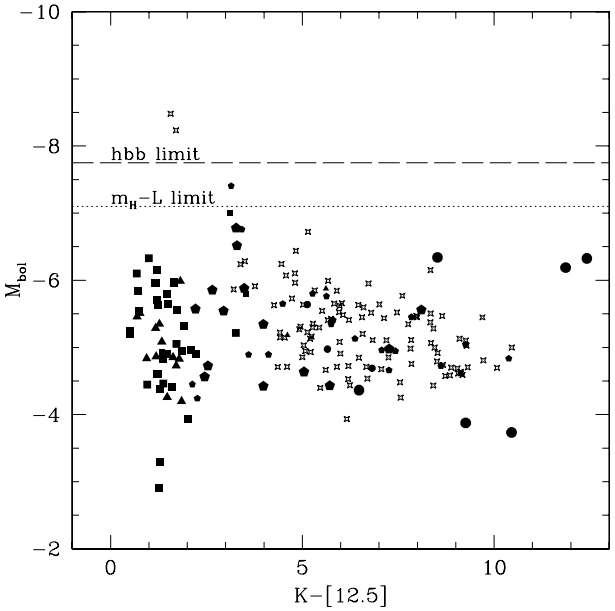

Fig. 9. The HR diagram of observed C stars adopting as a temperature indicator the near-to-mid IR colour K–[12.5], where contributions from both the photosphere and dust are present.

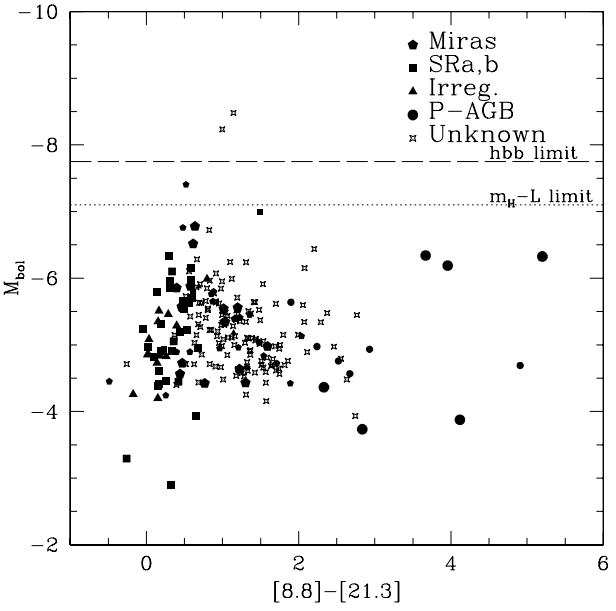

Fig. 10. The HR diagram of observed C stars in mid-IR, adopting the mid-IR colour [8.8]–[21.3] as abscissa.

for their low weight in the initial mass function and for the very short duration of the theoretically permitted phases. We can further notice that in Fig. 9 all the points representing known AGB stars with reliable distance estimates (large dots) stay (with one exception) below the limit for moderately massive stars ($M \leq 5\,M_{\odot}$); points beyond this level can therefore be simply explained as due to erroneous classifications (C-rich supergiants, e.g. of Wolf-Rayet type). Alternatively, they might be AGB stars whose luminosity has been overestimated due to poor distances or to uncertainties induced by variability.

HR-like diagrams can be constructed also using mid IR colours that include the effects of dust. An example is in Fig. 9: it shows that there are no semiregulars or irregulars for K–[12.5] ≥ 3 and no Miras for K–[12.5] ≤ 2; large IR excesses are associated to Mira variability or to post-AGB stars, or to unknown objects near the AGB end. Probably, the spread in magnitudes for any colour is also an outcome of a spread in stellar masses.

An interesting piece of information is added by Fig. 10, where the HR diagram is constructed using a purely mid-IR colour as abscissa. Here we are looking only at dust, photospheres should not be seen: we don't expect much further reddening on the emission from dust, which re-radiates the stellar flux. Indeed, the area covered by known long period variables is now quite small, defining a narrow sequence for sources along the AGB, and a limited colour extension of some more evolved sources, with a maximum colour for Miras of [8.8]–[21.3] = 2. All known stars redder than this are post-AGB objects; some unknown sources observed by MSX are present in the reddest area, and we suggest that they be classified as stars at the termination of the AGB stage or above it, in evolution toward the ejection of a planetary nebula. Large values of the mid-IR colours are in fact expected when the relatively warm dust of AGB stars becomes cooler, forming the extended (and often detached) shells of post-AGB stars.

6. Mass loss

Consider now Fig. 11 (panel a); it shows the relation between mass loss rates and bolometric magnitudes. In panel a, referring to irregulars, semiregulars and Miras, there is a general increase of mass loss rates with luminosity, which cannot however be reduced to a simple analytical formula (as examples, power-law relationships with three representative exponents have been added). The fact is that mass loss rates and luminosity should be correlated as, while becoming more luminous, AGB stars become also increasingly cool, their pulsation becomes stronger and both facts should power more intense stellar winds. The spread in panel a, partially confusing the relation, should then be ascribed to the presence of other variables, possibly the mass, and/or the fact that different mechanisms power stellar winds in different evolutionary stages. This evolutionary hypothesis was suggested by VL2 and van Loon et al. (2005) as the cause of a spread similar to the one we show; they in particular indicated that a switch from single scattering (Jura 1984) to multiple scattering (Gail & Sedlmayr 1986) of photons on dust grains as the star evolves can explain mass loss rates in excess of the momentum of radiation L/c. Notice that the points representing Miras stay in the upper part of the diagram, showing a steeper dependence of mass loss rates on luminosity. A sharp steepening of mass loss rates, up to a final superwind phase, is in fact necessary to let the whole envelope be ejected before the AGB termination. Including post-AGB stars and unknown sources in the plot, as done in Fig. 11, panel b, introduces further complexities. We believe we have here two problems. On one side, as already mentioned, the reddest objects radiate part of their flux at wavelengths longer than 45 μm, so that the luminosity we estimate for them is only a lower

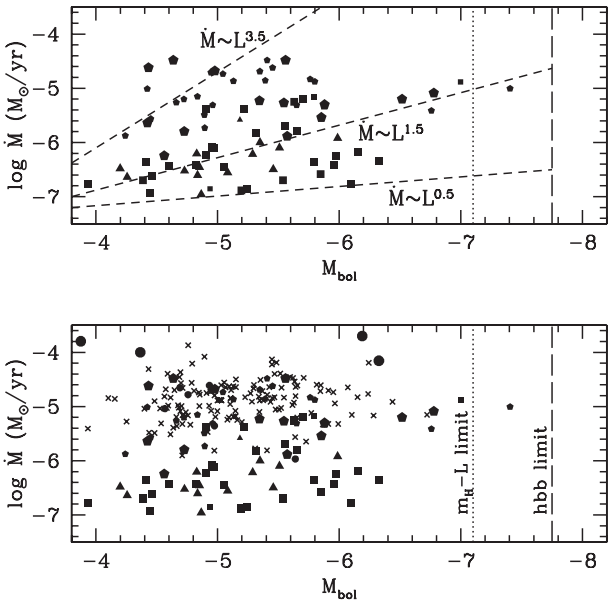

Fig. 11. *Top panel*: the bolometric magnitudes for AGB C-rich stars of known variability type, as indicated, plotted as a function of mass loss rates. *Bottom panel*: same as before, but including unknown and post-AGB sources.

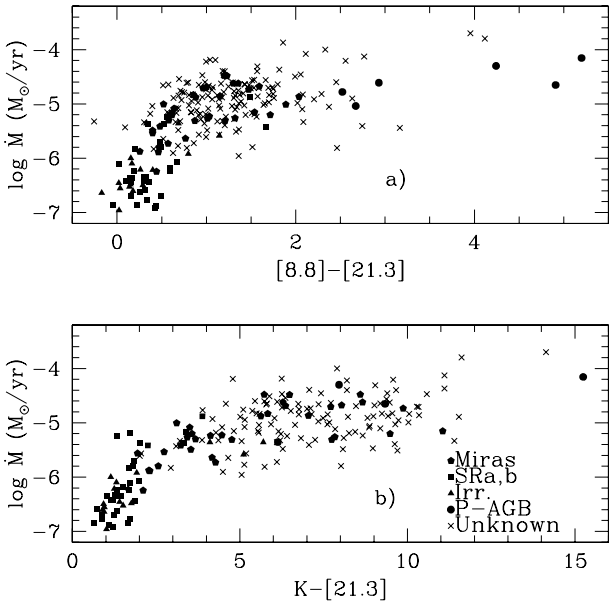

Fig. 12. Relations linking the mass loss rates of C-rich AGB and post-AGB sources to the IR colours up to 21 μm.

limit. On the other side, these sources are leaving (or have just left) the AGB and should have huge circumstellar envelopes with possibly detached shells escaping our spatial resolution. Any correlation is then hampered by poor spatial and/or spectral coverage.

A good monitor of the mass loss rate is instead available from the IR colours. This is illustrated in Fig. 12. In particular, when mid-IR colours are used, especially if including the 21.3 μm (with the characteristic emission feature of C-rich post-AGB stars), then the variation of mass loss rates with the stellar classes (and with evolution, if the hypothesis that Miras are on average quite evolved holds) is clearly distinguishable (panel a). All known long period variables remain at values of the [8.8]−[21.3] μm colour below 2, while post-AGB objects display much redder colours, probably due to cold dust formation. Again, transition objects exist among the sources of unknown classification. A similar effect is seen from the K−[21.3] colour (panel b), but here the separation of post-AGB stars from the rest is less clear, and a rather continuous distribution is seen. In general, the growth of the IR excess linking Miras to post-AGBs seems to be rather smooth, with no obvious break (e.g. for the superwind phase that is expected to terminate the AGB evolution).

Data like those discussed in this paper might be useful to infer which part of the mass return to the interstellar medium is due to carbon stars. This would require to integrate the mass lost by AGB stars over an Initial Mass Function and a Star Formation Rate for low and intermediate mass stars and to estimate the fractional contribution of carbon-rich phases. We shall therefore reconsider this task in a subsequent issue of this analysis, after M giants are included in the discussion.

7. Conclusions

In this paper we have presented the first issue of a series of works on the IR properties of galactic AGB and post-AGB stars, based on archived data from the 2MASS, MSX (6C Point Source Catalogue) and ISO-SWS experiments. In particular, we analyzed a sample of more than 230 C-rich AGB stars, for which estimates of distances, mass loss rates and colours from 1 to 21 (and sometimes 45) μm could be collected. We found that uncertainties still affect distances, except for a limited subset of objects with astrometric-quality data. Many sources were found to be extremely red, with SEDs extending to wavelengths unreachable by ground-based observations: in particular, we showed that, starting from the Mira stage, AGB carbon stars begin to radiate most of their flux beyond 10 μm. This excludes the possibility of deriving meaningful results on AGB luminosities by extrapolating fluxes obtained at optical or near-IR wavelengths (a practice that is unfortunately common even today). Using the best group of data, for which reliable distances and the whole SEDs up to 45 μm were available, we derived precise bolometric corrections, to be applied to the other sources, and thus we constructed the colour–magnitude diagrams in near and mid IR. The results suggest that AGB carbon stars of the Galaxy are objects of moderate mass (below about 5 $M_{\odot}$), and reach bolometric magnitudes between −4.5 and −6.4. These findings confirm (at a higher metallicity and with larger statistics) previous suggestions on Magellanic Clouds by other authors. The luminosities derived are in good agreement with those predicted by stellar models using the Schwarzschild's criterion for convection and are at odd with the belief (still persisting in some theoretical studies and population-synthesis works), according to which observed C-star luminosities would be lower than predicted by canonical stellar evolution.

We also analyzed mass loss rates and their relation with the magnitudes: we suggested that correlations between mass loss and luminosity are hard to derive for post-AGB objects, probably due to insufficient spatial and spectral coverage of their emission. For AGB stars instead, correlations of mass loss rates with luminosity exist, but reveal dependence by more than one parameter. Here the stellar mass and the activation of different mechanisms for powering mass loss should add their effects. Clearer correlations emerged between the mass loss rates and the IR colours, especially when the baseline was sufficiently extended in wavelength. These correlations also provided tools for classifying the evolutionary status of carbon stars.

Acknowledgements. We thank the referee, Dr J.Th. van Loon, for an extensive and helpful review, containing very relevant scientific advice. We also thank N. Epchtein, O. Straniero and A. Chieffi for many clarifying discussions. R.G. and M.B. acknowledge support in Italy by MIUR, under contract PRIN2004-025729. The IRAIT project is an Italo-French-Spanish collaboration funded in Europe by Polar and Astronomical Agencies (in Italy by Programma Nazionale delle Ricerche in Antartide and Istituto Nazionale di Astrofisica).
This research has made use of the SIMBAD database and the VizieR service (CDS, Strasbourg, France), and the IRSA (NASA/IPAC InfraRed Science Archive) database (USA). In particular archived data from the experiments MSX, ISO-SWS and 2MASS were used. • The processing of the science data of the Midcourse Space Experiment (MSX) was funded by the US Ballistic Missile Defense Organization with additional support from NASA Office of Space Science. • The Infrared Space Observatory (ISO) is an ESA project with instruments funded by ESA Member States (especially the PI countries: France, Germany, The Netherlands and UK) and with the participation of ISAS and NASA. • 2MASS (Two Micron All Sky Survey) is a joint project of the Univ. of Massachusetts and the Infrared Processing and Analysis Center (IPAC) at California Institute of Technology, funded by NASA and the NSF (USA).

References

Abia, C., Busso, M., Gallino, R., et al. 2001, ApJ, 559, 1117
Abia, C., Domínguez, I., Gallino R., et al. 2002, ApJ, 579, 817
Andersen, A. C., Höfner, S., & Gautschhy-Loidl, R. 2003, A&A, 400, 981
Bains, I., Bryce, M., Mellema, G., et al. 2003, MNRAS, 340, 381
Barnbaum, C., Zuckerman, B., & Kastner, J. H. 1991, AJ, 102, 289
Battinelli, P., & Demers, S. 2004a, A&A, 417, 479
Battinelli, P., & Demers, S. 2004b, A&A, 418, 33
Baumert, J. H. 1972, Ph.D. Thesis, The Ohio State University, Dissertation Abstracts International, Vol. 33−11, Sect. B, p. 5113
Bergeat, J., Knapik, A., & Rutily, B. 2001, A&A, 369, 178
Bergeat, J., Knapik, A., & Rutily, B. 2002a, A&A, 390, 967, (BKR1)
Bergeat, J., Knapik, A., & Rutily, B. 2002b, A&A, 390, 987, (BKR2)
Bergeat, J., & Chevallier, L. 2005, A&A, 429, 235
Bessell, M. S., Castelli, F., & Plez, B. 1998, A&A, 333, 231
Blanco, V. M., Blanco, B. M., & McCarthy, M. F. 1980, ApJ, 242, 938
Blöcker, T. 1995, A&A, 297, 727
Busso, M., Origlia, L., Marengo, M., et al. 1996, A&A, 311, 253
Busso, M., Gallino, R., & Wasserburg, G. J. 1999, ARA&A, 37, 239
Busso, M., Gallino, R., Lambert, D. L., et al. 2001, ApJ, 557, 802
Carciofi, A. C., Bjorkman, J. E., & Magalhães, A. M. 2004, ApJ, 604, 238
Cesarsky, C. J., Abergel, A., Agnese, P., et al. 1996, A&A, 315, 32
Cioni, M.-R. L., Marquette, J.-B., Loup, C., et al. 2001, A&A, 377, 945
Cioni, M.-R. L., Blommaert, J. A. D. L., Groenewegen, M. A. T., et al. 2003, A&A, 406, 51
Claussen, M. J., Kleinmann, S. G., Joyce, R. R., & Jura, M. 1987, ApJS, 65, 385
Cohen, M., Wheaton, Wm. A., & Megeath, S. T. 2003, AJ, 126, 1090
Costa, E., & Frogel, J. A. 1996, AJ, 112, 2607
Cox, J. P., & Giuli, R. T. 1968, Principles of Stellar Structure (New York: Gordon and Breach), 1968
Cutri, R. M., Skrutskie M. F., van Dyk S., et al. 2003, VizieR On-line Data Catalog: II/246, University of Massachusetts and Infrared Processing and Analysis Center, (IPAC/California Institute of Technology)
Demers, S., Battinelli, P., & Letarte, B. 2004, A&A, 424, 125
Domínguez, I., Chieffi, A., Limongi, M., & Straniero, O. 1999, ApJ, 524, 226
Draine, B. T. 1989, Infrared Spectroscopy in Astronomy, Proc. of the 22nd Eslab Symp., Salamanca, Spain, 1988, ed. B. H. Kaldeich. ESA SP-290, 93
Epchtein, N. 1999, IAUS 191, 97
Epchtein, N., Deul, E., Derriere, S., et al. 1999, A&A, 349, 236
Fleischer, A. J., Guager, A., & Sedlmayr, E. 1992, A&A, 266, 321
Fleischer, A. J., Guager, A., & Sedlmayr, E. 1995, A&A, 297, 543
Fouqué, P., Chevallier, L., Cohen, M., et al. 2000, A&AS, 141, 313
Frost, C. A., & Lattanzio, J. C. 1996, ApJ, 473, 383
Frost, C. A., Cannon, R. C., Lattanzio, J. C., et al. 1998, A&A, 332, 17
Gail, H.-P., & Sedlmayr, E. 1986, A&A, 161, 201
Gail, H.-P., & Sedlmayr, E. 1987, A&A, 171 197
Gallino, R., Arlandini, C., Busso M., et al. 1998, ApJ, 497, 388
Gezari, D. Y., Schmitz, M., Pitts, P. S., & Mead, J. M. 1993, Catalog of Infrared Observations, third edition
Gillett, F. C., Jones, T. W., Merrill, K. M., & Stein, W. A. 1975, A&A, 45, 77
Glass, I. S. 1999, The Handbook of Infrared Astronomy (Cambridge, England: Cambridge University Press)
Groenewegen, M. A. T., & Whitelock, P. A. 1996, MNRAS, 281, 1347
Groenewegen, M. A. T., & de Jong, T. 1998, A&A, 337, 797
Groenewegen, M. A. T., Sevenster, M., Spoon, H. W. W., & Pérez I. 2002a, A&A, 390, 501
Groenewegen, M. A. T., Sevenster, M., Spoon, H. W. W., & Pérez I. 2002b, A&A, 390, 511
Habing, H. J. 1996, A&AR, 7, 97
Herwig, F. 2005, ARA&A, in press
Hony, S., Tielens, A. G. G. M., Waters, L. B. F. M., & de Koter, A. 2003, A&A, 402, 211
Iben, I., & Renzini, A. 1983, ARA&A, 21, 271
Jaminet, P. A., Danchi, W. C., Sutton, E. C., et al. 1991, ApJ, 380, 461
Jura, M. 1984, ApJ, 282, 200
Jura, M., & Helfland, D. J. 1984, ApJ, 287, 785
Jura, M. 1986, ApJ, 303, 327
Jura, M., & Kleinmann, S. G. 1989, ApJ, 341, 359
Kahane, C., Dufour, E., Busso, M., et al. 2000, A&A, 357, 669
Karakas, A. I. 2003, Ph.D. Dissertation, Monash University
Karakas, A. I., & Lattanzio, J. C. 2003, PASA 20, 393
Karakas, A. I., & Lattanzio, J. C. 2004, Origin and Evolution of the Elements, from the Carnegie Observatories Centennial Symposia, Carnegie Observatories Astrophysics Series, ed. A. McWilliam & M. Rauch, Pasadena: Carnegie Observatories, 31
Kastner, J. H. 1992, ApJ, 401, 337
Kastner, J. H., Forveille, T., Zuckerman, B., & Omont, A. 1993, A&A, 275, 163

Kastner, J. H., & Soker, N. 2003, AAS 203, 3101
Knapik, A., Bergeat, J., & Rutily, B. 1999, A&A, 344, 263
Knapp, G. R., & Morris, M. 1985, ApJ, 292, 640
Knapp, G. R., Pourbaix, D., Platais, I., & Jorissen, A. 2003, A&A, 403, 993
Knude, J. 1979, A&A, 71, 344
Le Bertre, T. 1992, A&AS, 94, 377
Le Bertre, T. 1993, A&AS, 97, 729
Le Bertre, T., & Winters, J. M. 1998, A&A, 334, 173
Le Bertre, T., Matsuura, M., Winters, J. M., et al. 2001, A&A, 376, 997
Le Bertre, T., Tanaka, M., Yamamura, I., & Murakami, H. 2003, A&A, 403, 943
Loup, C., Forveille, T., Omont, A., & Paul, J. F. 1993, A&AS, 99, 291
Marengo, M., Canil, G., Silvestro, G., et al. 1997, A&A, 322, 924
Marengo, M., Busso, M., Silvestro, G., et al. 1999, A&A, 348, 501
Marengo, M., Ivezic, Z., & Knapp, G. R. 2001, MNRAS, 324, 1117
Marigo P., Girardi L., & Chiosi C. 2003, A&A, 403, 225
Meixner, M., Campbell, M. T., Welch, W. J., & Likkel, L. 1998, ApJ, 509, 392
Men'shchikov, A. B., Schertl, D., Tuthill, P. G., et al. 2002, A&A, 393, 867
Olivier, E. A., & Wood, P. R. 2003, ApJ, 584, 1035
Olofsson, H., Eriksson, K., Gustafsson, B., & Carlstrom, U. 1993a, ApJS, 87, 267
Olofsson, H., Eriksson, K., Gustafsson, B., & Carlstrom, U. 1993b, ApJS, 87, 305
Olofsson, H., González Delgado, D., Keschbaum, F., & Schöier, F. L. 2002, A&A, 391, 1053
Olofsson, A. O. H., Olofsson, G., Hjalmarson, Å., et al. 2003, A&A, 402, 47
Omont, A., Gilmore, G. F., Alard, C., et al. 2003, A&A, 403, 975
Ortiz, R., Lorenz-Martins, S., Maciel, W. J., & Rangel, E. M. 2005, A&A, 431, 565
Ott, U. 2001, Planetary and Space Science 49, 763
Pacźynski, B. 1975, ApJ, 202, 558
Persi, P., Ferrari-Toniolo, M., Marenzi, A. R., et al. 1994, Experimental Astron. 5, 363
Phillips, J. P. 1998, A&A, 340, 527
Sahai, R., & Liechti, S. 1995, A&A, 293, 198
Sahai, R., Kastner, J. H., Frank, A., et al. 2003, ApJ, 599, 87
Salpeter, E. E. 1974, ApJ, 193, 585
Samus, N. N., Durlevich, O. V., et al. 2004, VizieR On-line Data Catalog: II/250, Institute of Astronomy of Russian Academy of Science and Sternberg, State Astronomical Institute of the Moscow State University
Sandin, C., & Höfner, S. 2003a, A&A, 398, 253
Sandin, C., & Höfner, S. 2003b, A&A, 404, 789
Schirrmacher, V., Woitke, P., & Sedlmayr, E. 2003, A&A, 404, 267
Schöier, F. L., & Olofsson, H. 2001, A&A, 368, 969
Schöier, F. L., Ryde, N., & Olofsson, H. 2002, A&A, 391, 577
Sedlmayr, E. 1994, Lect. Notes Phys., 428, 163
Skinner, C. J., Meixner, M., Barlow, M. J., et al. 1997, A&A, 328, 290
Smith, V. V., Plez, B., Lambert, D. L., & Lubowich, D. A. 1995, ApJ, 441, 735
Stancliffe, R. J., Izzard, R. G., & Tout, C. A. 2005, MNRAS, 356, 1
Straniero, O., Chieffi, A., Limongi, M., et al. 1997, ApJ, 478, 332
Straniero, O., Chieffi, A., & Limongi, M. 1998, Proc. of the 9th workshop on Nuclear Astrophysics, ed. W. Hillebrandt and E. Muller, Garching bei Munchen: Max-Planck-Institut fur Astrophysik, 42
Straniero, O., Limongi, M., Chieffi, A., et al. 2000, MmSAI 71, 719
Straniero, O., Domínguez, I., Cristallo, S., & Gallino, R. 2003, PASA 20, 389
Straniero, O., Gallino, R., & Cristallo, S. 2005, Nucl. Phys. A, in press
Tosti, G., Busso, M., Straniero, O., et al. 2004, Proc. SPIE, 5489, 742
Valentijn, E. A., Feuchtgruber, H., Kester, D. J. M., et al. 1996, A&A, 315, 60
Van Eck, S., Jorissen, A., Udry, S., et al. 1998, A&A, 329, 971
van Loon, J. Th., Zijlstra, A. A., Whitelock, P. A., et al. 1997, A&A, 325, 585
van Loon, J. Th., Zijlstra, A. A., Whitelock, P. A., et al. 1998, A&A, 329, 169
van Loon, J. Th., Zijlstra, A. A., & Groenewegen, M. A. T. 1999a, A&A, 346, 805, (VL1)
van Loon, J. Th., Groenewegen, M. A. T., de Koter, A., et al. 1999b, A&A, 351, 559, (VL2)
van Loon, J.Th., Zijlstra, A. A., Kaper, L., et al. 2001, A&A, 368, 239
van Loon, J. Th., Cioni, M.-R. L., Zijlstra, A. A., & Loup C. 2005, A&A, 438, 273
van Winckel, H., & Reyniers, M. 2000, A&A, 354, 135
Vassiliadis, E., & Wood, P. R. 1993, ApJ, 413, 641
Wachter, A., Schröder, K.-P., Winters, J. M., et al. 2002, A&A, 384, 452
Wagenhuber, J., & Groenewegen, M. A. T. 1998, A&A, 340, 183
Wasserburg, G. J., Busso, M., Gallino, R., & Nollett K. M. 2005, Nucl, Phys. A (in press)
Whitelock, P. A., Feast, M. W., van Loon, J. Th., & Zijlstra, A. A. 2003, MNRAS, 342, 86
Winters, J. M., Dominik, C., & Sedlmayr, E. 1994a, A&A, 288, 255
Winters, J. M., Fleischer, A. J., Gauger, A., & Sedlmayr, E. 1994b, A&A, 290, 623
Winters, J. M., Fleischer, A.J., Le Bertre, T., & Sedlmayr, E. 1997, A&A, 326, 305
Winters, J. M., Keady, J. J., Gauger, A., & Sada, P. V. 2000a, A&A, 359, 651
Winters, J. M., Le Bertre, T., Jeong, K. S., et al. 2000b, A&A, 361, 641
Winters, J. M., Le Bertre, T., Nyman, L.-Å., et al. 2002, A&A, 388, 609
Winters, J. M., Le Bertre, T., Jeong, K. S., et al. 2003, A&A, 409, 715
Wood, P. R. 1996, MmSAI, 67, 691
Wood, P. R., & Sebo, K. M. 1996, MNRAS, 282, 958
Wood, P. R., Alcock, C., Allsman, R. A., et al. 1999, IAUS, 191, 151
Wood, P. R. 2000, PASA, 17, 18
Wood, P. R., & Cohen, M. 2001, Post-AGB Objects as a Phase of Stellar Evolution, Proceedings of the Torun Workshop held July 5–7, 2000. ed. R. Szczerba & S.K. Górny. Astrophysics and Space Science Library Boston, Dordrecht, London, Kluwer Academic Publishers, 265, 71
Wood, P. R. 2003, Mass-losing pulsating stars and their circumstellar matter. Workshop, May 13–16, 2002, Sendai, Japan, ed. Y. Nakada, M. Honma and M. Seki. Astrophysics and Space Science Library (Dordrecht: Kluwer Academic Publishers), 283, 3
Wood, P. R., Olivier, E. A., & Kawaler, S. D. 2004, ApJ, 604, 800
Zinner, E. 2000, Meteoritics & Planetary Science Suppl. 35, A177

Online Material

Table 1. Relevant data of our sample of carbon stars with astrometric, or reliable, distance estimates. Here and in next tables the following rules apply for labelling. i) For the variability type, M means Mira; S means Semiregular; I means Irregular (P is used for all Post-AGB stars, "-" for all stars of unknown variability). ii) References for mass loss are quoted in the following way: B: stands for Bergeat & Chevallier (2005); L is for Loup et al. (1993); G is for Groenewegen et al. (2002b); Mei1998 is for Meixner et al. (1998); Men2002 for Men'shchikov et al. (2002); S1997 for Skinner et al. (1997); Jam1991 for Jaminet et al. (1991). iii) References for distance are: B for Bergeat & Chevallier (2005); L for Loup et al. (1993); G for Groenewegen et al. (2002b); S for Schöier & Olofsson (2001), using methods from Groenewegen et al. (2002b); S* for the same authors, when using methods from Loup et al. (1993); Mei1998 for Meixner et al. (1998); Men2002 for Men'shchikov et al. (2002); S1997 for Skinner et al. (1997); Hon2003 for Hony et al. (2003); Bains2003 for Bains et al. (2003); Phill1998 for Phillips (1998); K: method by Kastner (1992).

IRAS name	Other name	Var. type	Mass Loss [$M_\odot$/yr]	Type ref.	v [km/s]	d [kpc]	Type ref.	J [Jy]	H [Jy]	K [Jy]	8.8 [Jy]	11.7 [Jy]	12.5 [Jy]	14.6 [Jy]	21.3 [Jy]	Data origin
02270−2619	R For	M	5.00E-06	B	16.5	0.86	B	32.4	99.0	193	277	262	196	133	80.4	ISO
03229+4721	V384 Per	M	5.90E-06	B	15.0	0.72	B	21.6	93.7	231	451	527	373	264	199	ISO
04504+4949	AU Aur	M	5.70E-07	B	–	1.47	B	13.2	27.5	45.0	16.4	–	16.7	6.1	4.2	MSX
05185+3227	UV Aur	M	1.60E-06	B	10.0	1.09	B	39.0	63.5	93.8	50.5	–	37.8	22.2	13.3	MSX
06342+0328	V688 Mon	M	2.40E-05	B	13.4	1.37	B	0.27	2.6	12.9	106	–	103	88.8	60.0	MSX
08088−3243	V346 Pup	M	3.31E-05	B	20.7	1.12	B	1.5	8.2	33.7	177	–	144	141.2	93.1	MSX
09452+1330	CW Leo	M	3.30E-05	B	14.7	0.15	B	2.7	74.9	469	35332	37100	33545	26309	18194	ISO
12447+0425	RU Vir	M	2.30E-06	B	18.4	0.68	B	9.7	27.2	82.2	157	172	133	91.6	54.3	ISO
15477+3943	V CrB	M	1.30E-06	B	7.5	0.84	B	65.0	134	198	90.0	99.6	62.5	37.7	23.5	ISO
17556+5813	T Dra	M	8.20E-06	B	13.5	1.43	B	37.8	107	190	220	243	159	105	67.6	ISO
20396+4757	V Cyg	M	6.30E-06	B	11.5	0.74	B	92.1	317	599	758	771	512	345	228	ISO
21320+3850	V1426 Cyg	M	5.40E-06	B	14.0	0.82	B	71.9	193	310	238	–	193	150.7	103.3	MSX
21358+7823	S Cep	M	2.90E-06	B	22.0	0.50	B	178	403	685	490	455	325	215	121	ISO
23320+4316	LP And	M	2.10E-05	B	14.0	0.84	B	0.23	2.9	19.1	599	750	631	516	442	ISO
01246−3248	R Scl	S	6.40E-06	B	16.9	0.47	B	–	540	743	172	136	93.5	63.1	50.9	ISO
03374+6229	U Cam	S	2.00E-06	B	20.6	0.53	B	189	385	417	120	119	85.6	54.9	32.0	ISO
03377+5120	V466 Per	S	2.40E-07	B	9.0	0.53	B	132	266	308	69.3	–	45.0	28.4	15.0	MSX
04127+5030	SY Per	S	1.50E-06	B	17.5	1.43	B	23.1	62.7	93.6	30.8	–	22.5	10.8	6.3	MSX
04491+3825	V346 Aur	S	2.00E-07	B	–	1.11	B	91.7	192	185	20.8	–	14.3	7.1	5.6	MSX
05028+0106	W Ori	S	3.80E-07	B	11.0	0.41	B	489	941	1028	190	186	124	80.5	43.1	ISO
05238+3406	S Aur	S	4.20E-06	B	25.5	1.13	B	17.8	57.1	112	123	–	93.5	58.4	34.3	MSX
05421+2424	TU Tau	S	5.70E-07	B	–	1.05	B	74.1	149	156	33.6	32.1	28.1	19.7	9.9	ISO
05426+2040	Y Tau	S	1.60E-06	B	11.0	0.74	B	242	495	481	136	–	77.8	59.1	36.4	MSX
06077+2601	TU Gem	S	4.40E-07	B	11.5	0.52	B	171	327	313	76.7	–	56.4	29.9	15.3	MSX
06192+0722	BN Mon	S	4.20E-06	B	24.2	1.28	B	24.9	59.1	78.6	30.4	–	25.4	11.2	7.1	MSX
06197+0327	FU Mon	S	2.60E-07	B	–	1.45	B	69.9	148	143	16.2	–	10.6	3.8	3.7	MSX
06315+1606	CR Gem	S	8.40E-07	B	14.9	0.92	B	59.2	158	162	44.8	–	36.7	15.6	14.2	MSX
06556+0614	RV Mon	S	1.70E-07	B	–	0.67	B	59.0	112	126	26.5	–	31.5	14.7	8.2	MSX
06585−0310	V614 Mon	S	1.50E-08	B	–	0.48	B	81.6	122	131	26.8	–	16.5	9.0	3.6	MSX
07045−0728	RY Mon	S	5.90E-07	B	11.0	0.69	B	132	255	277	66.2	–	44.6	24.5	13.5	MSX
08525+1725	X Cnc	S	6.20E-07	B	7.0	0.71	B	376	653	629	–	–	–	–	–	–
–	Y Hya	S	3.70E-07	B	9.0	0.49	B	200	364	413	90.5	–	52.1	35.1	17.9	MSX
09582−5958	SZ Car	S	4.60E-07	B	14.0	0.37	B	83.2	146	153	30.1	–	20.1	9.2	6.9	MSX
12226+0102	SS Vir	S	3.60E-07	B	12.5	0.56	B	81.9	193	310	103	105	62.2	34.4	24.6	ISO
12427+4542	Y CVn	S	1.40E-07	B	8.5	0.26	B	641	1331	1316	205	162	85.7	53.8	33.5	ISO
12544+6615	RY Dra	S	4.40E-07	B	10.0	0.55	B	218	425	464	127	93.6	73.1	50.4	24.7	ISO
15096−6009	AS Cir	S	7.80E-07	B	–	0.93	B	56.6	134	167	62.5	–	44.9	21.6	10.9	MSX
17441−3541	SX Sco	S	3.80E-07	B	–	0.83	B	91.4	181	185	37.8	–	25.4	14.2	7.1	MSX
18476−0758	S Sct	S	5.60E-06	B	17.3	0.58	B	191	358	374	63.1	53.5	48.2	28.0	18.0	ISO
19017−0545	V Aql	S	6.60E-07	B	8.5	0.56	B	281	575	740	144	117	93.6	66.4	42.2	ISO
19390+3229	TT Cyg	S	1.20E-07	B	13.5	0.62	B	52.6	99.4	110	19.1	12.8	10.9	7.5	4.8	ISO
20115+3834	RS Cyg	S	2.00E-07	B	–	0.65	B	83.2	165	198	41.8	–	24.9	14.3	8.2	MSX
21168−4514	T Ind	S	1.70E-07	B	6.0	0.65	B	257	419	397	53.7	38.7	30.7	22.9	12.5	ISO
21399+3516	V460 Cyg	S	4.50E-07	B	10.0	0.64	B	303	599	520	84.6	67.9	53.5	34.6	19.1	ISO
23587+6004	WZ Cas	S	1.30E-07	B	3.8	0.65	B	182	330	353	53.5	30.1	23.4	18.3	13.7	ISO
03075+5742	V623 Cas	I	1.10E-07	B	–	0.51	B	114	213	219	43.1	29.3	25.4	19.4	7.5	ISO
05449+3036	FU Aur	I	2.80E-07	B	–	1.29	B	49.5	92.0	96.4	17.6	–	12.8	6.2	3.1	MSX
06225+1445	BL Ori	I	2.50E-07	B	9.0	0.60	B	212	405	328	52.7	–	32.1	18.6	10.6	MSX
07057−1150	W CMa	I	6.10E-07	B	10.5	0.79	B	178	298	295	53.6	–	35.8	23.5	13.2	MSX
12465−6129	RX Cru	I	6.20E-07	B	–	0.85	B	65.7	149	182	52.1	–	36.7	18.7	11.3	MSX
17172−4020	V1079 Sco	I	1.20E-06	B	–	0.92	B	88.2	214	264	58.2	86.7	54.8	30.1	20.7	ISO
18040−0941	FX Ser	I	3.10E-05	B	28.4	1.23	B	2.2	13.3	55.4	–	–	–	–	–	–
18155−1327	ES Ser	I	3.00E-07	B	–	0.91	B	53.1	119	145	40.2	–	27.1	15.0	7.8	MSX
18306+3657	T Lyr	I	8.00E-07	B	11.5	0.65	B	187	430	504	121	69.4	41.9	29.9	24.0	ISO
18448+0523	DR Ser	I	1.00E-06	B	20.1	1.29	B	46.7	104	123	23.9	–	15.4	7.7	4.7	MSX
19147+2149	CG Vul	I	3.30E-07	B	–	0.81	B	41.1	87.2	112	38.8	–	23.9	14.1	7.6	MSX
21553+5015	LW Cyg	I	3.50E-07	B	–	1.09	B	36.0	81.3	110	31.1	–	19.2	9.3	5.4	MSX
22423+6127	DG Cep	I	2.30E-07	B	–	0.80	B	48.8	102	119	26.1	–	18.0	9.0	3.8	MSX
23438+0312	TX Psc	I	3.20E-07	B	10.7	0.32	B	529	1038	1065	160	103	82.8	60.4	35.5	ISO
04395+3601	RAFGL 618	P	2.00E-04	Mei1998	19.5	1.70	Mei1998	< 0.01	0.03	0.20	193	400	450	651	1260	ISO
06176−1036	Red Rectangle	P	1.00E-04	Men2002	5.0	0.71	Men2002	3.7	9.0	23.0	323	380	369	377	472	ISO
–	RAFGL 2688	P	7.00E-05	S1997	19.5	1.20	S1997	< 0.01	0.19	0.19	170	619	749	1253	3496	ISO
–	NGC 7027	P	1.60E-04	Jam1991	18.6	0.65	Bains2003	0.23	1.0	1.6	133	357	332	447	1005	ISO
21282+5050	–	P	–	–	–	2.00	Mei1998	0.04	0.05	0.10	27.9	60.7	61.4	64.1	64.8	ISO
21306+4422	IC 5117	P	–	–	–	10.23	Phill1998	0.05	0.05	0.11	6.7	12.9	11.4	14.3	33.5	ISO

Table 2. Relevant data for AGB C stars of known variability type with non-astrometric distances.

IRAS name	Other name	Var. type	Mass Loss [$M_\odot$/yr]	Type ref.	v [km/s]	d [kpc]	Type ref.	J [Jy]	H [Jy]	K [Jy]	8.8 [Jy]	11.7 [Jy]	12.5 [Jy]	14.6 [Jy]	21.3 [Jy]	Data origin
01080+5327	HV Cas	M	3.23E-06	G	22.6	0.97	S	9.3	27.9	68.8	103	104	77.7	51.4	25.3	ISO
02293+5748	V596 Per	M	9.75E-06	L	14.2	2.04	G	< 0.01	< 0.01	< 0.01	72.0	101	82.7	69.2	70.0	ISO
05405+3240	V370 Aur	M	2.40E-05	L	28.0	2.01	G	0.05	0.53	3.6	248	–	202	227.5	147.8	MSX
06226−0905	V636 Mon	M	5.80E-06	L	25.2	0.88	L	8.2	29.5	73.2	159	150	108	73.9	46.2	ISO
06268+0849	V477 Mon	M	1.33E-05	L	33.0	3.36	G	0.55	2.6	9.7	64.0	–	51.2	38.0	24.6	MSX
06447+0817	V840 Mon	M	1.47E-05	G	24.4	4.62	G	0.23	1.1	4.1	33.1	–	29.9	19.8	12.4	MSX
06529+0626	CL Mon	M	2.73E-06	L	26.1	0.77	S	26.8	79.9	144	112	–	42.2	16.5	12.2	MSX
11514−5841	V875 Cen	M	1.84E-05	G	17.8	3.80	G	0.15	0.13	0.22	41.2	–	44.8	35.4	27.3	MSX
18240+2326	V1076 Her	M	6.30E-06	L	16.1	0.92	G	0.01	0.33	3.8	404	478	437	367	335	ISO
18397+1738	V821 Her	M	6.44E-06	L	14.2	0.90	G	8.2	42.9	134	–	–	–	–	–	–
18398−0220	V1417 Aql	M	1.39E-05	L	35.3	0.95	G	0.02	0.04	0.04	378	414	332	251	187	ISO
19248+0658	V1421 Aql	M	4.90E-06	G	16.1	2.02	G	2.2	8.9	24.0	71.8	84.6	61.6	42.2	27.3	ISO
19321+2757	V1965 Cyg	M	1.36E-05	L	25.7	1.36	G	0.41	3.5	16.7	140	–	243	240.1	155.7	MSX
19419+3222	V1991 Cyg	M	3.87E-06	G	19.4	3.85	G	12.7	24.3	38.3	40.3	–	36.9	19.1	10.7	MSX
19537+2212	V359 Vul	M	1.86E-06	G	15.1	1.47	G	3.0	11.7	37.5	94.2	–	68.3	46.1	27.2	MSX
19559+3301	KL Cyg	M	9.90E-06	G	18.6	4.57	G	11.7	30.8	53.0	47.9	–	39.5	23.4	13.2	MSX
20072+3116	V1969 Cyg	M	2.05E-05	G	25.6	1.76	G	0.81	5.4	17.9	207	–	147	129.5	89.0	MSX
21366+4529	V1568 Cyg	M	5.34E-06	G	20.2	2.31	G	0.82	3.2	8.8	36.2	–	–	–	–	MSX
21377+5042	V2345 Cyg	M	4.91E-06	G	18.0	2.29	G	0.09	0.68	3.1	106	–	86.4	73.9	55.3	MSX
21440+7324	PQ Cep	M	1.33E-06	L	21.7	0.39	S	66.8	183	288	155	147	95.0	57.4	33.4	ISO
21449+4950	V2358 Cyg	M	5.48E-06	L	17.3	3.11	G	0.02	0.19	1.1	37.5	–	36.9	26.3	21.6	MSX
22241+6005	V384 Cep	M	3.29E-05	L	34.2	1.96	G	0.44	3.8	14.8	155	–	127	117.3	82.1	MSX
23257+1038	IZ Peg	M	7.04E-06	L	10.1	1.61	G	< 0.01	0.03	0.29	151	194	167	130	106	ISO
23491+6243	V955 Cas	M	1.96E-05	G	21.7	3.71	G	0.02	0.15	0.91	37.7	–	34.8	23.5	15.6	MSX
00172+4425	VX And	S	1.40E-07	B	11.5	0.56	S	84.7	179	222	68.5	43.5	31.7	23.1	14.4	ISO
18234−2206	V2548 Sgr	S	1.31E-05	G	23.8	2.90	G	25.5	63.0	90.9	68.5	–	66.6	45.3	46.0	MSX
18401+2854	FI Lyr	S	3.82E-06	L	12.3	0.88	L	244	365	345	49.0	67.0	62.3	46.6	39.0	ISO
21070+4711	V573 Cyg	S	6.83E-06	G	21.1	3.26	G	4.8	12.9	21.2	22.6	–	22.6	10.6	6.8	MSX
07270−1921	V569 Pup	I	4.40E-06	L	25.5	1.10	L	6.0	18.2	47.6	127	–	83.5	53.3	29.5	MSX
21035+5136	V1549 Cyg	I	2.61E-06	L	11.4	1.30	G	2.2	13.8	50.9	163	–	146	128.2	79.9	MSX
23174+5941	V571 Cas	I	4.40E-06	L	14.5	4.58	G	0.26	1.4	4.6	38.9	–	33.7	19.5	12.5	MSX
01144+6658	V829 Cas	P	2.45E-05	L	18.2	2.79	G	0.01	0.02	0.01	43.3	75.0	82.3	96.3	110	ISO
07134+1005	HD 56126	P	2.23E-05	L	10.7	2.40	Hon2003	2.9	2.1	1.5	7.4	29.7	33.2	42.0	116	ISO
08544−4431	–	P	1.08E-06	G	8.2	1.98	G	9.5	13.1	25.9	137	–	121	143.6	134.2	MSX
19008+0726	V1418 Aql	P	4.41E-06	L	18.2	0.95	G	1.4	9.5	46.0	137	–	346	363.5	184.6	MSX
21318+5631	RAFGL 5625S	P	1.66E-05	L	16.9	1.77	G	0.03	0.03	0.02	110	178	169	174	192	ISO
22272+5435	V354 Lac	P	5.00E-05	K	10.6	2.35	L	11.3	11.3	10.5	26.7	99.4	95.4	97.6	227	ISO
23166+1655	LL Peg	P	9.12E-06	L	14.1	1.00	G	0.09	0.09	0.07	268	408	441	507	535	ISO
03192+5642	KX Cam	M	–	–	–	–	–	0.61	3.0	8.2	25.1	–	24.6	12.5	9.2	MSX
–	IY Hya	I	–	–	–	–	–	6.8	35.0	109	293	–	222	197.8	117.3	MSX
05251−1244	ZZ Lep	P	–	–	–	–	–	0.19	0.13	0.16	9.9	40.8	47.0	37.9	119	ISO
07027−7934	GLMP 170	P	–	–	–	–	–	0.03	0.09	0.32	20.2	21.2	19.5	27.5	61.7	ISO
17028−1004	Butterfly Nebula	P	–	–	–	–	–	0.05	0.22	1.1	33.4	43.3	41.4	40.0	52.5	ISO
17047−5650	V837 Ara	P	–	–	–	–	–	0.25	0.41	1.2	130	157	152	138	247	ISO
19327+3024	V1966 Cyg	P	–	–	–	–	–	0.30	0.21	0.38	50.3	94.3	106	96.8	198	ISO
19454+2920	GLMP 950	P	–	–	–	–	–	0.03	0.05	0.05	3.6	13.8	22.2	41.9	85.6	ISO
19477+2401	GLMP 952	P	–	–	–	–	–	0.01	0.05	0.10	4.0	–	17.3	19.1	34.3	MSX
19480+2504	GLMP 953	P	–	–	–	–	–	< 0.01	< 0.01	< 0.01	7.6	18.9	19.8	30.5	41.1	ISO
20000+3239	GLMP 963	P	–	–	–	–	–	0.99	1.5	1.6	7.3	19.2	19.5	21.9	51.7	ISO
23304+6147	GLMP 1078	P	–	–	–	–	–	0.63	0.75	0.69	5.0	15.3	15.4	16.9	51.2	ISO

Table 3. Relevant data for AGB C stars of unknown variability type and with non-astrometric distances. First part.

IRAS name	Other name	Var. type	Mass Loss [$M_\odot$/yr]	Type ref.	v [km/s]	d [kpc]	Type ref.	J [Jy]	H [Jy]	K [Jy]	8.8 [Jy]	11.7 [Jy]	12.5 [Jy]	14.6 [Jy]	21.3 [Jy]	Data origin
01105+6241	NSV 438	–	1.48E-06	L	23.3	0.67	S*	20.3	74.9	160	136	–	89.3	62.1	33.9	MSX
01142+6306	CGCS 201	–	2.09E-05	L	16.5	4.49	G	< 0.01	0.02	0.16	16.7	–	20.0	12.8	9.0	MSX
01443+6417	RAFGL 248	–	1.75E-05	G	30.5	2.49	G	1.6	6.5	13.0	61.6	–	49.7	32.8	20.2	MSX
03096+5839	CGCS 458	–	9.40E-06	L	14.0	4.90	L	0.12	0.57	1.9	12.9	–	14.9	8.2	6.3	MSX
03277+5120	–	–	5.63E-06	G	17.1	4.93	G	0.14	0.67	2.6	12.9	–	13.1	6.4	–	MSX
03293+6038	–	–	3.49E-05	G	21.0	3.61	G	< 0.01	0.02	0.20	–	–	35.2	22.1	16.8	MSX
03301+5658	–	–	1.98E-05	L	17.0	6.98	G	< 0.01	< 0.01	0.10	25.9	–	30.2	22.7	18.1	MSX
03313+6058	–	–	8.81E-06	L	13.9	5.24	G	< 0.01	< 0.01	< 0.01	25.3	35.4	33.5	33.1	38.4	ISO
03385+5927	–	–	6.45E-06	G	16.5	3.21	G	0.01	0.13	0.92	61.8	–	51.2	35.3	26.3	MSX
04340+4623	RAFGL 6316S	–	1.48E-05	L	15.5	4.22	G	< 0.01	0.05	0.44	50.3	–	51.2	41.9	30.4	MSX
04369+4501	–	–	1.46E-05	G	20.9	4.92	G	0.14	0.82	3.1	21.2	–	20.8	11.8	7.6	MSX
04449+4951	–	–	8.86E-06	G	40.0	2.07	G	2.4	9.4	19.1	51.5	–	–	–	–	MSX
04530+4427	RAFGL 6319S	–	1.46E-05	L	20.2	2.60	G	< 0.01	0.03	0.35	62.5	–	63.9	62.0	51.2	MSX
06183+1135	RAFGL 918	–	1.25E-06	G	18.6	1.84	G	2.4	8.7	18.3	53.3	–	41.7	25.7	16.2	MSX
06206+0931	CGCS 1252	–	2.26E-06	L	10.0	3.22	G	0.98	4.6	13.0	48.8	–	41.6	20.5	13.4	MSX
06238+0904	RAFGL 940	–	7.05E-06	L	16.0	3.86	G	0.57	3.2	11.7	74.2	78.9	55.1	39.9	27.1	ISO
06344−0124	–	–	1.04E-05	G	17.7	5.05	G	–	< 0.01	–	11.6	–	18.9	14.0	12.7	MSX
06462−4157	–	–	2.73E-06	G	7.6	4.53	G	116	176	172	32.9	–	30.0	20.1	16.1	MSX
06471+0301	RAFGL 1017	–	7.02E-06	G	19.9	3.42	G	1.1	5.5	15.7	65.7	–	54.0	30.8	18.8	MSX
06487+0551	RAFGL 1020	–	1.69E-06	G	11.0	2.59	G	0.93	4.6	12.3	61.3	–	48.2	31.4	19.6	MSX
06505−0450	–	–	6.27E-06	L	12.0	5.00	G	0.01	0.01	0.01	25.4	–	28.9	21.6	16.3	MSX
06531−0216	RAFGL 1039	–	4.60E-06	L	29.0	1.30	L	0.72	3.2	11.1	73.3	–	47.6	29.7	16.5	MSX
06564+0342	RAFGL 5215	–	6.26E-06	L	9.9	3.49	G	0.28	1.5	5.8	63.7	–	50.8	34.9	25.2	MSX
06582+1507	–	–	2.52E-05	L	14.7	4.70	G	–	–	< 0.01	41.4	62.1	62.8	62.5	67.6	ISO
07080−0106	–	–	9.20E-06	G	25.4	3.63	G	0.04	0.30	1.5	17.4	–	18.6	10.3	9.7	MSX
07085−0018	RAFGL 5225	–	3.38E-05	G	20.3	3.87	G	0.12	0.91	4.2	45.5	–	41.9	27.1	18.7	MSX
07170+0721	–	–	5.20E-06	G	17.6	3.94	G	0.05	0.36	1.9	34.9	–	32.5	20.8	14.1	MSX
07217−1246	RAFGL 5230	–	4.36E-06	L	24.9	1.86	G	0.48	2.6	9.3	86.5	–	66.8	48.7	36.3	MSX
07368−2833	–	–	2.50E-05	G	19.7	3.86	G	0.15	1.1	4.7	23.7	–	24.5	14.9	10.0	MSX
07434−1847	–	–	1.53E-05	L	14.5	5.29	G	< 0.01	< 0.01	< 0.01	10.9	–	15.9	10.3	9.3	MSX
07546−2551	–	–	1.61E-05	G	20.2	6.26	G	0.10	0.31	–	17.9	–	17.4	8.9	6.1	MSX
08050−2838	RAFGL 5240	–	6.56E-06	L	15.0	2.55	G	0.29	2.2	9.4	56.0	–	46.9	31.2	22.5	MSX
08074−3615	–	–	1.29E-05	L	17.3	2.10	G	< 0.01	0.01	0.24	160	–	148	159.6	137.6	MSX
08086−3905	–	–	1.97E-05	G	17.0	4.44	G	< 0.01	< 0.01	0.06	25.5	–	32.3	24.8	20.7	MSX
08119−3627	–	–	8.37E-06	G	19.0	2.83	G	0.35	1.8	6.9	34.6	–	30.5	17.7	11.1	MSX
08191−3653	–	–	1.11E-05	L	18.0	4.31	G	< 0.01	0.01	0.18	32.0	–	36.8	26.3	19.6	MSX
08305−3314	–	–	1.35E-04	G	28.7	4.21	G	< 0.01	< 0.01	0.03	18.2	–	29.7	18.6	17.2	MSX
08340−3357	RAFGL 5251	–	9.11E-06	G	22.5	1.91	G	0.17	1.3	7.4	72.5	–	47.1	20.8	17.8	MSX
08353−3424	–	–	4.77E-06	G	22.0	2.54	G	0.68	2.9	8.7	50.5	–	24.7	12.3	6.8	MSX
08534−5055	–	–	4.91E-05	G	26.6	3.10	G	< 0.01	0.03	0.37	30.1	–	35.7	28.5	21.8	MSX
08535−4724	–	–	6.85E-06	G	17.1	3.17	G	< 0.01	0.08	0.76	37.2	–	42.8	33.8	25.5	MSX
09176−5147	–	–	1.06E-05	G	23.7	3.28	G	0.02	0.19	1.2	36.6	–	32.3	21.2	14.4	MSX
09178−5556	–	–	4.00E-05	G	20.1	6.40	G	< 0.01	0.05	0.33	16.8	–	20.6	11.4	8.7	MSX
09317−5116	–	–	2.29E-05	G	11.4	4.37	G	< 0.01	< 0.01	< 0.01	35.5	–	45.7	39.7	31.7	MSX
09496−5050	–	–	2.78E-05	G	25.4	4.62	G	< 0.01	< 0.01	0.04	23.5	–	32.3	20.6	16.5	MSX
09513−5324	–	–	2.02E-05	G	20.0	1.97	G	0.04	0.43	2.7	206	–	153	135.6	94.3	MSX
09533−6021	–	–	2.20E-05	G	19.9	4.51	G	0.02	0.15	0.84	37.9	–	16.2	12.6	10.4	MSX
10098−5742	–	–	1.29E-05	G	15.2	4.02	G	0.01	0.13	0.87	42.0	–	45.3	35.6	23.9	MSX
11073−6325	–	–	7.62E-06	G	11.8	5.40	G	0.01	0.13	0.79	40.0	–	36.2	22.2	15.5	MSX
11145−6534	–	–	1.66E-05	G	18.5	1.83	G	0.41	3.8	15.7	93.9	–	64.9	30.8	31.3	MSX
11186−5528	–	–	1.03E-05	G	17.2	1.45	G	1.4	5.6	24.1	97.2	–	121	90.3	–	MSX
12142−6410	–	–	6.43E-05	G	34.0	5.25	G	1.0	3.9	8.9	21.9	–	22.1	14.0	10.3	MSX
12298−5754	RAFGL 4151	–	1.81E-05	G	20.2	2.02	G	0.13	0.91	5.4	107	–	87.1	71.2	48.8	MSX
12397−6447	–	–	3.38E-05	G	24.5	5.29	G	0.05	0.10	0.09	46.2	–	44.3	32.4	23.7	MSX
12419−6058	–	–	3.17E-05	G	15.2	3.36	G	< 0.01	< 0.01	0.04	54.2	–	67.3	69.1	57.9	MSX
12562−6003	–	–	1.42E-05	G	18.5	4.24	G	–	0.12	0.96	26.2	–	29.6	20.9	15.1	MSX
12595−6035	–	–	4.06E-05	G	16.6	6.53	G	0.01	0.13	0.78	14.6	–	16.7	10.2	7.4	MSX
13031−5743	–	–	4.79E-06	G	10.9	3.41	G	2.1	8.2	20.1	30.9	–	26.6	14.4	10.1	MSX
13045−6404	–	–	1.95E-05	G	13.6	3.77	G	< 0.01	0.01	0.11	30.9	–	37.5	31.4	22.7	MSX
13343−5807	–	–	4.77E-06	G	13.0	3.13	G	0.38	2.5	10.7	95.3	–	81.8	61.7	45.7	MSX
13509−6348	–	–	4.06E-06	G	8.3	3.00	G	0.14	0.27	0.27	51.2	–	48.9	36.6	26.5	MSX
14404−6320	–	–	8.22E-06	G	16.8	3.33	G	< 0.01	0.05	0.53	53.2	–	52.3	39.1	26.3	MSX
14443−5708	–	–	2.72E-05	G	26.6	4.09	G	< 0.01	0.02	0.19	21.7	–	27.4	19.5	14.9	MSX
14484−6152	RAFGL 4202	–	3.92E-06	G	19.0	0.57	G	0.97	7.9	36.1	160	–	432	523.3	341.8	MSX
14521−6058	–	–	2.28E-05	G	24.8	4.25	G	0.14	0.87	3.3	33.8	–	27.0	15.2	9.8	MSX
15043−5438	–	–	6.94E-06	G	17.9	2.32	G	0.15	1.0	5.2	58.3	–	49.4	34.6	21.4	MSX
15054−5458	–	–	6.19E-05	G	21.4	5.25	G	0.08	0.16	0.16	8.9	–	17.5	17.2	16.0	MSX
15084−5702	–	–	9.55E-06	L	26.0	2.75	G	< 0.01	< 0.01	< 0.01	63.0	–	66.9	63.1	48.6	MSX
15471−5644	–	–	1.26E-05	G	21.7	2.41	G	0.03	0.04	0.04	45.7	–	70.6	91.1	88.1	MSX
15488−4928	–	–	2.23E-05	G	22.6	2.75	G	0.50	2.7	7.6	80.8	–	75.7	67.0	53.9	MSX
16079−4812	–	–	2.26E-05	G	14.5	2.08	G	< 0.01	0.13	1.6	165	–	141	141.9	105.4	MSX
16123−4654	–	–	9.41E-06	G	11.7	4.28	G	0.01	0.18	1.1	49.1	–	44.8	29.0	17.6	MSX
16171−4759	–	–	2.17E-05	G	23.3	3.14	G	0.31	1.8	6.4	42.4	–	39.4	27.8	18.6	MSX
16296−4417	–	–	1.32E-05	G	19.6	4.41	G	< 0.01	< 0.01	< 0.01	29.8	–	34.9	26.5	20.0	MSX
16298−5349	–	–	1.92E-05	G	20.2	4.76	G	0.15	0.97	3.5	37.8	–	33.3	22.6	15.9	MSX
16304−3831	–	–	2.47E-06	G	9.7	4.83	G	67.4	122	121	25.5	–	23.9	15.5	10.9	MSX
16469−4753	–	–	1.49E-05	G	17.5	5.27	G	< 0.01	0.11	0.67	54.2	–	59.7	57.6	62.7	MSX
16562−5039	–	–	6.32E-06	G	19.7	2.62	G	0.13	0.74	3.5	50.7	–	42.9	25.3	–	MSX

Table 4. Relevant data for AGB C stars of unknown variability type and with non-astrometric distances. Second part.

IRAS name	Other name	Var. type	Mass Loss [$M_\odot$/yr]	Type ref.	v [km/s]	d [kpc]	Type ref.	J [Jy]	H [Jy]	K [Jy]	8.8 [Jy]	11.7 [Jy]	12.5 [Jy]	14.6 [Jy]	21.3 [Jy]	Data origin
17050−4642	–	–	6.42E-06	G	11.7	5.44	G	< 0.01	< 0.01	< 0.01	12.1	–	16.7	11.5	8.5	MSX
17079−3243	–	–	1.49E-05	G	25.6	1.55	G	1.9	7.5	29.0	174	–	135	110.6	64.9	MSX
17217−3916	–	–	1.60E-06	L	8.8	2.40	L	< 0.01	0.18	1.7	55.6	–	59.3	49.2	38.3	MSX
17278−3937	–	–	6.82E-06	G	27.7	3.32	G	4.7	13.7	32.5	34.3	–	33.6	16.9	10.8	MSX
17309−3412	–	–	1.56E-05	G	16.8	5.24	G	0.07	0.25	0.62	41.2	–	43.8	38.3	25.8	MSX
17375−3652	RAFGL 5369	–	4.29E-05	G	22.5	2.65	G	< 0.01	< 0.01	0.16	68.1	–	69.4	72.7	61.8	MSX
17547−3249	–	–	1.07E-05	G	12.0	5.90	G	0.08	0.10	0.08	26.1	–	33.1	27.5	21.3	MSX
17581−1744	RAFGL 2047	–	1.14E-05	L	19.7	2.85	G	1.6	7.8	19.8	87.6	–	68.6	48.1	32.2	MSX
17583−2201	–	–	3.60E-06	L	12.4	2.90	L	< 0.01	0.02	0.03	9.4	–	23.5	27.9	29.6	MSX
18030−1707	–	–	1.33E-05	G	17.4	5.27	G	0.05	0.10	0.11	21.9	–	23.0	12.9	9.0	MSX
18036−2344	RAFGL 5440	–	3.09E-05	G	21.7	2.25	G	0.21	2.9	14.3	86.5	–	76.0	66.8	45.8	MSX
18100−1420	–	–	5.80E-06	L	18.0	3.70	L	0.22	0.62	0.80	69.8	–	67.1	53.9	36.6	MSX
18119−2244	RAFGL 2096	–	8.22E-06	G	17.8	2.45	G	0.01	0.21	–	140	–	109	93.4	61.1	MSX
18147−2215	RAFGL 2110	–	2.31E-05	G	20.9	3.40	G	0.01	0.26	2.8	75.2	–	72.5	65.1	47.8	MSX
18156−0653	RAFGL 2118	–	6.62E-06	G	20.0	1.69	G	2.2	9.9	31.7	96.7	–	76.5	45.6	23.2	MSX
18239−0655	RAFGL 2154	–	1.77E-05	L	27.0	1.64	G	0.16	1.9	11.9	143	–	122	118.7	85.4	MSX
18244−0108	–	–	4.64E-06	G	16.8	3.23	G	3.1	9.6	25.3	22.1	–	20.0	9.2	6.9	MSX
18244−0815	–	–	1.22E-05	L	21.5	3.93	G	0.03	0.25	1.6	48.3	–	46.0	31.4	22.0	MSX
18248−0839	–	–	3.08E-06	L	16.1	2.10	G	< 0.01	0.05	0.56	104	–	97.3	84.6	60.4	MSX
18269−1257	–	–	7.86E-06	L	19.5	3.06	G	< 0.01	0.04	0.41	48.0	–	49.9	39.7	27.7	MSX
18301−0656	–	–	1.10E-06	L	20.0	1.80	L	4.7	13.5	20.8	51.7	–	55.4	41.9	30.9	MSX
18320−0352	RAFGL 7012S	–	1.93E-05	L	22.5	3.67	G	< 0.01	< 0.01	< 0.01	73.0	–	71.3	65.8	49.4	MSX
18356−0951	–	–	1.43E-05	G	28.2	3.16	G	0.10	–	–	29.6	–	32.0	19.6	12.9	MSX
18367−0452	–	–	5.80E-06	L	16.0	2.50	L	< 0.01	0.01	0.01	46.8	–	52.1	44.2	33.6	MSX
18369−1034	–	–	8.77E-06	L	13.5	4.75	G	< 0.01	0.05	0.45	38.5	–	40.5	28.3	22.6	MSX
18400−0704	–	–	3.38E-06	L	14.5	4.57	G	0.11	0.23	0.24	22.5	–	26.0	17.8	13.5	MSX
18424+0346	–	–	1.43E-05	L	20.0	3.17	G	0.13	0.78	3.6	80.8	–	62.9	43.3	26.0	MSX
18464−0656	RAFGL 2256	–	4.62E-06	G	15.4	2.94	G	< 0.01	< 0.01	0.10	43.5	56.9	58.2	55.6	50.7	ISO
18475+0926	RAFGL 2259	–	9.39E-06	L	21.8	1.62	G	0.02	0.14	1.1	176	–	156	161.8	111.6	MSX
19029+0839	–	–	1.90E-06	L	25.0	2.00	L	0.05	0.47	2.3	24.2	–	23.5	14.0	9.1	MSX
19029+0808	RAFGL 2316	–	1.31E-05	L	17.0	2.90	G	< 0.01	0.08	1.1	119	–	96.3	87.8	60.0	MSX
19068+0544	–	–	1.71E-05	L	20.5	3.25	G	2.9	13.7	39.1	34.9	44.6	36.5	26.2	19.9	ISO
19108+1155	–	–	1.29E-05	G	26.6	3.05	G	0.30	1.8	6.6	30.8	–	27.9	16.1	9.4	MSX
19238+1159	–	–	7.97E-06	G	16.2	3.83	G	< 0.01	< 0.01	< 0.01	47.7	–	65.0	71.4	54.9	MSX
19253+1918	–	–	2.35E-05	G	25.0	5.54	G	< 0.01	0.02	0.03	18.7	–	23.3	15.4	11.0	MSX
19296+2227	–	–	1.22E-05	G	11.4	5.10	G	1.7	5.7	9.5	26.7	–	33.4	32.0	34.7	MSX
19304+2529	–	–	1.54E-06	G	16.5	4.73	G	< 0.01	< 0.01	< 0.01	16.8	–	29.6	30.6	27.7	MSX
19346+1209	–	–	1.84E-05	L	13.3	4.57	G	0.05	0.43	2.5	57.4	–	50.1	36.0	24.5	MSX
19417+3053	–	–	1.02E-05	G	18.8	5.15	G	0.02	0.12	0.49	13.5	–	16.0	10.6	8.1	MSX
19457+2346	RAFGL 2457S	–	2.36E-05	G	22.0	3.89	G	< 0.01	0.03	0.26	44.6	–	45.8	33.9	22.2	MSX
19485+3235	–	–	2.48E-05	G	20.5	4.66	G	0.05	0.09	0.08	27.9	–	30.4	21.5	15.7	MSX
19523+2414	–	–	2.89E-05	G	22.2	5.20	G	0.02	0.29	1.7	26.3	–	27.0	15.1	8.5	MSX
19524+2130	–	–	2.25E-05	G	21.2	5.50	G	0.46	2.4	6.6	15.9	–	18.2	8.9	6.3	MSX
19548+3035	RAFGL 2477	–	7.44E-05	L	33.7	3.38	G	0.13	0.26	0.28	49.7	84.1	85.5	95.3	108	ISO
19552+3142	–	–	1.23E-05	G	27.2	4.21	G	< 0.01	0.07	0.45	42.9	–	42.4	30.1	20.9	MSX
19558+3333	–	–	1.90E-05	G	19.2	4.22	G	< 0.01	< 0.01	0.01	32.6	–	35.2	33.6	27.8	MSX
20014+2830	–	–	2.74E-05	G	22.4	5.21	G	< 0.01	< 0.01	0.02	14.2	–	19.9	14.1	11.2	MSX
20159+3134	–	–	6.48E-05	G	28.3	5.24	G	0.02	0.27	1.9	19.1	–	20.7	12.5	8.5	MSX
20200+3624	–	–	1.18E-05	G	23.5	3.96	G	0.51	3.1	9.6	19.3	–	20.0	10.2	6.4	MSX
20204+2914	–	–	1.44E-05	G	15.8	3.97	G	0.01	0.17	1.4	29.8	–	31.3	19.9	14.3	MSX
20282+3604	–	–	1.55E-06	G	18.2	3.35	G	0.19	1.4	5.5	43.7	–	41.5	24.9	15.3	MSX
20311+4222	RAFGL 2604	–	4.87E-06	G	13.1	2.15	G	0.02	0.37	3.1	68.7	–	61.0	53.8	34.8	MSX
20323+3153	–	–	2.73E-06	G	14.0	4.01	G	0.36	1.9	6.7	28.5	–	28.0	16.2	11.3	MSX
20435+3825	–	–	3.26E-06	L	20.6	1.90	G	0.02	0.30	2.1	114	–	88.3	77.2	49.4	MSX
20461+4817	–	–	6.00E-05	G	31.2	5.64	G	< 0.01	0.06	0.40	25.3	–	26.1	17.5	10.8	MSX
20596+3833	–	–	2.16E-05	G	27.4	4.00	G	0.03	0.26	1.4	30.3	–	–	–	–	MSX
21003+4801	–	–	5.72E-06	L	14.8	2.62	G	0.09	0.93	5.5	65.9	–	55.6	41.4	28.6	MSX
21088+4546	–	–	8.30E-06	G	18.9	4.02	G	0.29	1.6	5.3	14.7	–	14.3	6.8	4.6	MSX
21147+5110	–	–	1.38E-05	L	11.5	3.17	G	< 0.01	< 0.01	0.10	26.4	–	29.0	23.5	19.2	MSX
21265+5042	–	–	2.44E-05	G	23.2	5.61	G	0.04	0.44	2.0	22.3	–	21.0	12.6	7.8	MSX
21324+5537	–	–	4.01E-05	G	20.5	4.15	G	< 0.01	0.01	0.13	18.4	–	24.6	18.3	13.3	MSX
21373+4540	–	–	5.27E-06	L	14.7	2.27	G	0.02	0.18	1.2	49.6	–	50.2	39.5	28.3	MSX
21444+5053	–	–	3.50E-05	G	12.9	6.48	G	0.03	0.23	0.98	11.3	–	17.4	11.9	12.8	MSX
21489+5301	–	–	1.02E-05	L	21.5	2.51	G	< 0.01	0.02	0.31	58.3	85.0	68.6	49.3	45.7	ISO
22039+5328	–	–	3.30E-06	G	36.3	2.66	G	0.09	0.64	2.5	35.9	–	32.3	20.9	11.5	MSX
22125+5608	–	–	3.70E-06	L	25.5	2.40	L	2.9	9.7	16.3	21.6	–	17.1	7.2	4.0	MSX
22303+5950	–	–	1.52E-05	L	18.3	3.86	G	< 0.01	< 0.01	< 0.01	42.0	57.8	57.9	58.1	59.0	ISO
22354+5911	–	–	1.65E-05	L	20.0	6.44	G	0.02	0.19	1.1	11.9	–	13.4	7.1	6.1	MSX
22585+6402	RAFGL 3011	–	2.48E-05	L	21.4	2.37	G	1.1	6.5	19.9	156	–	110	87.2	55.3	MSX
23234+6434	–	–	8.32E-05	G	18.6	5.96	G	< 0.01	< 0.01	< 0.01	10.4	–	17.8	14.2	12.4	MSX
23516+6430	–	–	2.02E-05	G	18.1	4.02	G	< 0.01	< 0.01	0.08	20.8	–	28.6	22.1	17.6	MSX
00210+6221	–	–	–	–	–	–	–	0.01	0.02	0.02	13.0	19.5	20.3	21.2	24.0	ISO
06088+1909	RAFGL 6371S	–	–	–	–	2.68	G	0.91	4.5	13.5	39.8	–	32.4	21.8	14.6	MSX
17512−2548	RAFGL 2023	–	–	–	–	–	–	< 0.01	0.16	1.6	143	–	112	112.7	87.8	MSX
18491−0008	–	–	–	–	–	–	–	0.03	0.08	0.10	33.9	–	38.8	29.7	23.2	MSX
19075+0921	RAFGL 2333	–	–	–	–	–	–	< 0.01	0.04	0.07	108	–	140	176.0	142.4	MSX
22130+5634	–	–	–	–	–	–	–	< 0.01	< 0.01	0.03	16.6	–	22.1	15.9	12.3	MSX